



Measurements of Temperature and N₂ Number Density in the Combustion Cylinder of a Compression Ignition Engine Utilizing Laser-Raman Diagnostics

W. D. Williams, J. W. L. Lewis,
and J. H. Jones
ARO, Inc.

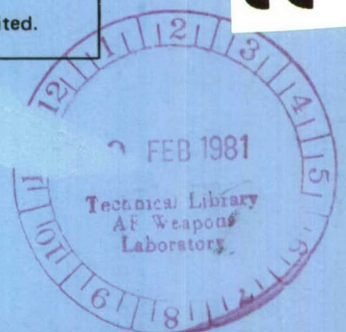
January 1981

Final Report for Period February 24, 1980 — October 1, 1980

LOAN COPY: RETURN TO
AFWL TECHNICAL LIBRARY
KIRTLAND AFB, N.M.

20080211214

Approved for public release; distribution unlimited.



**ARNOLD ENGINEERING DEVELOPMENT CENTER
ARNOLD AIR FORCE STATION, TENNESSEE
AIR FORCE SYSTEMS COMMAND
UNITED STATES AIR FORCE**

NOTICES

When U. S. Government drawings, specifications, or other data are used for any purpose other than a definitely related Government procurement operation, the Government thereby incurs no responsibility nor any obligation whatsoever, and the fact that the Government may have formulated, furnished, or in any way supplied the said drawings, specifications, or other data, is not to be regarded by implication or otherwise, or in any manner licensing the holder or any other person or corporation, or conveying any rights or permission to manufacture, use, or sell any patented invention that may in any way be related thereto.

Qualified users may obtain copies of this report from the Defense Technical Information Center.

References to named commercial products in this report are not to be considered in any sense as an indorsement of the product by the United States Air Force or the Government.

This report has been reviewed by the Office of Public Affairs (PA) and is releasable to the National Technical Information Service (NTIS). At NTIS, it will be available to the general public, including foreign nations.

APPROVAL STATEMENT

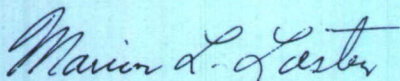
This report has been reviewed and approved.



KENNETH H. LENERS, Captain, USAF
Project Manager
Directorate of Technology

Approved for publication:

FOR THE COMMANDER



MARION L. LASTER
Director of Technology
Deputy for Operations

UNCLASSIFIED

REPORT DOCUMENTATION PAGE		READ INSTRUCTIONS BEFORE COMPLETING FORM
1. REPORT NUMBER AEDC-TR-80-55	2. GOVT ACCESSION NO.	3. RECIPIENT'S CATALOG NUMBER
4. TITLE (and Subtitle) MEASUREMENTS OF TEMPERATURE AND N ₂ NUMBER DENSITY IN THE COMBUSTION CYLINDER OF A CI ENGINE UTILIZING LASER-RAMAN DIAGNOSTICS		5. TYPE OF REPORT & PERIOD COVERED Final - Feb. 24, 1980 - Oct. 1, 1980
		6. PERFORMING ORG. REPORT NUMBER
7. AUTHOR(s) W. D. Williams, J. W. L. Lewis, and J. H. Jones, ARO, Inc., a Sverdrup Corporation Company		8. CONTRACT OR GRANT NUMBER(s)
9. PERFORMING ORGANIZATION NAME AND ADDRESS Arnold Engineering Development Center/DOT Air Force Systems Command Arnold Air Force Station, Tennessee 37389		10. PROGRAM ELEMENT, PROJECT, TASK AREA & WORK UNIT NUMBERS Program Elements 921C08 and 65807F
11. CONTROLLING OFFICE NAME AND ADDRESS Arnold Engineering Development Center/DOS Air Force Systems Command Arnold Air Force Station, Tennessee 37389		12. REPORT DATE January 1981
		13. NUMBER OF PAGES 43
14. MONITORING AGENCY NAME & ADDRESS (if different from Controlling Office)		15. SECURITY CLASS. (of this report) UNCLASSIFIED
		15a. DECLASSIFICATION/DOWNGRADING SCHEDULE N/A
16. DISTRIBUTION STATEMENT (of this Report) Approved for public release; distribution unlimited.		
17. DISTRIBUTION STATEMENT (of the abstract entered in Block 20, if different from Report)		
18. SUPPLEMENTARY NOTES Available in Defense Technical Information Center (DTIC).		
19. KEY WORDS (Continue on reverse side if necessary and identify by block number) <div style="display: flex; justify-content: space-between;"> <div> compression ignition engines combustion chamber gases diagnostic equipment gas analysis </div> <div> Raman spectra lasers spectrometers fuels </div> <div> nitrogen </div> </div>		
20. ABSTRACT (Continue on reverse side if necessary and identify by block number) Laser-Raman scattering has been used to measure temperature and nitrogen number density in the combustion cylinder of a specialized research CI engine. Measurements were made as a function of crank angle degrees (CAD) for unfueled operation at 500 and 1,000 rpm and for operation at 1,000 rpm using n-heptane as an alternate fuel to diesel fuel no. 2. A pulsed ruby laser system was the excitation source for the Raman scattering, and the CAD resolution of the		

UNCLASSIFIED

UNCLASSIFIED

20. ABSTRACT (Continued)

measurements was 1.5×10^{-4} to 0.36 degrees.

UNCLASSIFIED

AD-A094221

PREFACE

The work reported herein was conducted by the Arnold Engineering Development Center (AEDC), Air Force Systems Command (AFSC), for the U. S. Army Research Office under Program Elements 921C08 and 65807F. The results of the research were obtained by ARO, Inc., AEDC Group (a Sverdrup Corporation Company), operating contractor for the AEDC, AFSC, Arnold Air Force Station, Tennessee, under ARO Project No. P34M-20A. The Air Force project manager at AEDC was Capt. Kenneth H. Leners; the U.S. Army Research Office project manager was Mr. James J. Murray. The data analysis was completed on January 27, 1980, and the manuscript was submitted for publication on October 1, 1980.

CONTENTS

	<u>Page</u>
1.0 INTRODUCTION	5
2.0 DESCRIPTION OF APPARATUS AND OPERATION	
2.1 Diesel Engine	6
2.2 Laser System	13
2.3 Spectrometer System	14
2.4 Data Acquisition System	15
3.0 LASER-RAMAN MEASUREMENT TECHNIQUE	
3.1 Vibrational Relaxation Considerations	23
3.2 Spectra and Intensity Relations	26
3.3 Calibrations and Data Reduction	29
4.0 DISCUSSION	
4.1 Chronology of Experiments	32
4.2 Results	35
5.0 SUMMARY	38
REFERENCES	38

ILLUSTRATIONS

Figure

1. Diesel Cycle	7
2. Geometrical Relations for Volume-Crank Angle Equation	8
3. Photograph of TACOM Engine	10
4. Engine Timing Cycle	11
5. TACOM Engine Viewport Spacer	12
6. TACOM Engine Modified Piston	16
7. Diesel Engine Experimental Setup	17
8. Block Diagram of Conventional Mode Data Acquisition System	19
9. Timing Diagram for Conventional Mode Data Acquisition System	20
10. Block Diagram of Q-Switch Data Acquisition System	21
11. Timing Diagram of Q-Switch Data Acquisition System	22
12. Vibrational Relaxation as a Function of Crank Angle	25
13. N ₂ VIB-ROT Band, Laser Wavelength at 6943 Å	27
14. N ₂ VIB-ROT Band, Laser Wavelength at 3471.5 Å	28
15. R _v and C _F (T, N ₂) as a Function of Temperature	29

<u>Figure</u>	<u>Page</u>
16. $N_2 + O_2$ in Air Rayleigh Line and Pure Rotational Band, Laser Wavelength at 6943 \AA	30
17. Intensity Ratio, $I_c(7061 \text{ \AA})/I_c(7010 \text{ \AA})$, as a Function of Rotational Temperature ..	31
18. Variation of Normalized Temperature with Crank Angle for Unfueled Operation ...	33
19. Comparison of Laser-Induced Incandescence with Blackbody Emission	34
20. Temperature and N_2 Number Density as a Function of CAD	36

TABLE

1. Valve/Fuel Injection Timing	11
--------------------------------------	----

NOMENCLATURE	41
--------------------	----

1.0 INTRODUCTION

It is desirable to improve performance of internal combustion engine systems because of present and projected fuel availability and cost, as well as environmental considerations. Such an improvement requires a better understanding of the combustion process itself, and various areas of study, including both high- and low-pressure flame investigations, are available for this purpose. Although such studies are both necessary and productive for elucidating basic reaction mechanisms, their impact on actual engine design has been less than desired. As noted in Ref. 1, "design and development of combustion systems is done experimentally with maximum dependence on past experience and minimal use of theory." The "minimal use of theory" is a result of the complexity of the processes occurring within the combustion chamber of an engine. A complete analysis of the process would include complex reaction schemes, nonequilibrium transport phenomena, turbulence, the gas dynamics of two-phase flow processes, and spatially distributed wall heat transfer. Clearly, such *a priori* analysis is beyond current capabilities, and recourse must be made to experimental studies.

Experimental investigations may improve the understanding of the combustion process, and the continued development of nonintrusive, nonperturbing diagnostic techniques (Ref. 2) promises spatially and temporally resolved measurements of the temperature and relative species number densities within the combustion chamber. Specifically, when compression ignition engines are considered, attempts to model the diesel engine combustion processes, as typified by Refs. 3 through 5, require as input data the temperature and its spatial profile throughout the combustion chamber, and such data have only recently begun to be provided. Early attempts to obtain temperature data have included the use of the sodium line reversal technique (Ref. 6), the variation of the speed of sound (Ref. 7), dual wavelength infrared measurements (Ref. 8), the emission-absorption technique (Ref. 9), and spectral emission measurements (Refs. 10 and 11). Although these various techniques have achieved moderate success, spatial resolution has not been achieved because all such measurements yield, at best, a temperature value which has been integrated along a temperature- and density-variable optical or ray transmission "line-of-sight."

In contrast to these techniques, Raman scattering provides measurements of local, time resolved values of both the rotational and vibrational temperature, as well as the number density of molecular species. Recently, spontaneous Raman scattering has been used to obtain relative species concentrations in internal combustion engines such as the Wisconsin L-head engine (Ref. 12) and to obtain N_2 number densities and their fluctuations in a stratified charge engine (Ref. 13). Furthermore, coherent anti-Stokes Raman scattering (CARS) has been used recently to obtain temperature measurements within a Ricardo E6 engine fueled with both gasoline and propane (Ref. 14).

The use of Raman scattering for combustion diagnostics, and particularly combustion chamber studies, is attractive for many reasons, such as its molecular specificity and its ability to measure temperatures and density with a spatial resolution on the order of 10^{-3} cc or less, if desired. Further, this nonperturbing measurement method results from a photon-molecule scattering process which occurs with a characteristic time of less than 1 psec. Consequently, since the intermolecular collision time at a gas density of 10 amagat is on the order of 10 psec, the effects of molecular collisions on the incoherent scattering process are inconsequential.

Since extensive descriptions of the Raman scattering process have been presented in Refs. 15 and 16, only a brief summary will be given here. An intense, monochromatic laser beam incident within the combustion environment under investigation has a small fraction of its photons scattered from the beam, some of which are unshifted in wavelength (Rayleigh and Mie scattering) while some are shifted to both higher wavelengths (Raman Stokes scattering) and lower wavelengths (Raman anti-Stokes scattering). The magnitude of the wavelength shift depends on the individual molecular species of the combustion region, and the magnitude of the scattered intensity varies directly with the species number density. Furthermore, the spectral distribution of the scattered radiation corresponding to a particular species is a function of the gas temperature. Because the incident beam can interact with both the characteristic rotational or vibrational molecular motions, both pure rotational Raman scattering and rotational-vibrational scattering can be observed. The former interaction yields the rotational temperature (T_R) of the species while the latter interaction provides both T_R and the vibrational temperature (T_v) of the species. The type of scattering employed for diagnostic purposes depends on many considerations, and Refs. 17 and 18 demonstrate the use of both rotational and vibrational Raman scattering, respectively.

The objective of this work was to demonstrate the feasibility of using spontaneous Raman scattering to study a compression ignition (CI) engine. Specifically, this technique was to be used to determine the local values of the gas temperature and relative number density within the particulate-laden environment of a CI engine combustion cylinder. The data were to be acquired as a function of the engine crank angle throughout the compression and power strokes. Finally, measurements were desired for two types of diesel fuels such as diesel no. 2 and n-heptane.

2.0 DESCRIPTION OF APPARATUS AND OPERATION

2.1 Diesel Engine

Figure 1 shows the pressure (P) - volume (V) plane of the idealized diesel constant pressure cycle. For the four-stroke cycle shown in Fig. 1, the intake and compression strokes

are designated as $a \rightarrow b$ and $b \rightarrow c$, respectively. Combustion of the injected diesel fuel is assumed to occur isobarically as the $c \rightarrow d$ path shows, and the expansion stroke ($d \rightarrow e$) is followed by the valve exhaust ($e \rightarrow b$) and exhaust stroke ($b \rightarrow a$). The compression and expansion strokes are assumed to be adiabatic and the valve exhaust process is assumed to be isochoric. The ideal, constant pressure diesel process shown in Fig. 1 differs from the standard gasoline engine, or Otto, cycle only in the $c \rightarrow d$ heat addition path, which in the Otto cycle is an isochoric process.

The difference between the maximum and minimum volumes of the cycle, V_{\max} and V_{\min} , respectively, is defined as the displacement (\bar{D}). Additionally, the compression ratio (r) is defined by

$$r = \frac{V_{\max}}{V_{\min}} \quad (1)$$

so that the clearance (V_{\min}) of the engine is given by

$$V_{\min} = \frac{\bar{D}}{(r-1)} \quad (2)$$

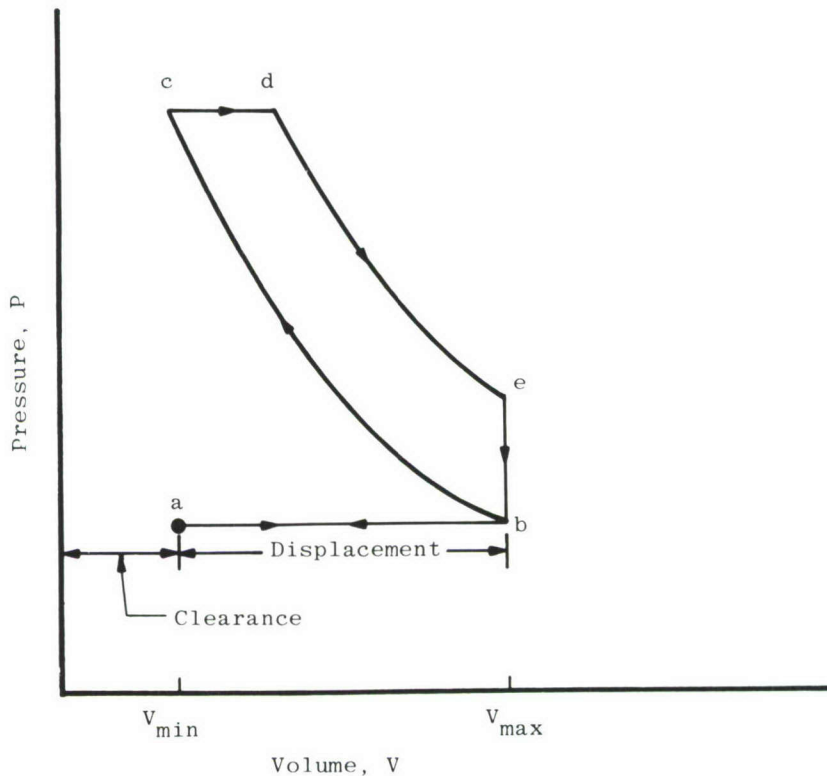


Figure 1. Diesel cycle.

Figure 2 shows the geometrical relationship between the crank angle, θ , and the linear displacement, s , of a piston of diameter D which is driven by a connecting rod of length ℓ' and a shaft crank radius r' . Figure 2 shows that the volume $V(\theta)$ for a given crank angle is

$$V(\theta) = V_o + Ar' \left\{ (1 - \cos \theta) + \left(\frac{\ell'}{r'} \right) \left[1 - \left\{ 1 - \left(\frac{r'}{\ell'} \right)^2 \sin^2 \theta \right\}^{1/2} \right] \right\} \quad (3)$$

where $V_o = V_{\min}$

and

$$A = \frac{\pi D^2}{4}$$

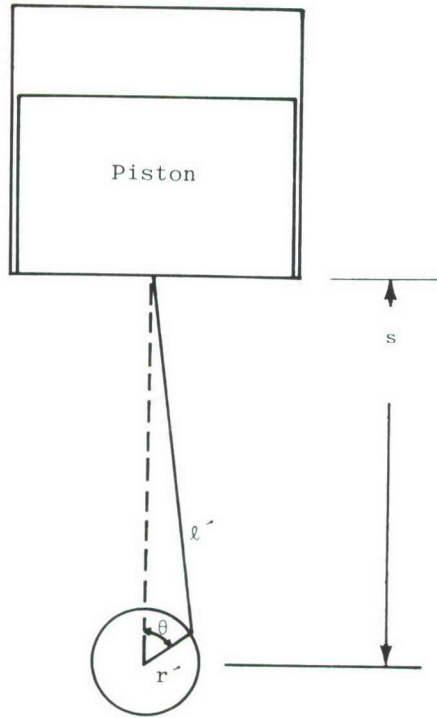


Figure 2. Geometrical relations for volume-crank angle equation.

For sufficiently small values of the ratio r'/ℓ' :

$$V(\theta) \approx V_o + Ar' \left[(1 - \cos \theta) + \left(\frac{r'}{4\ell'} \right) (1 - \cos 2\theta) \right] \quad (4)$$

and, using the relation

$$Ar' = (r-1) V_o / 2 \quad (5)$$

it is seen that

$$V(\theta) = V_o \left\{ 1 + \left[\frac{(r-1)}{2} \right] \left[(1-\cos \theta) + \left(\frac{r'}{4\ell'} \right) (1-\cos 2\theta) \right] \right\} \quad (6)$$

The CI engine used for these measurements was a single cylinder research engine manufactured by Labeco, Inc., for the Army Tank Automotive Command (TACOM). It was a four-stroke cycle engine with a 4.51 in. (11.46 cm) bore and a 4.5 in. stroke; the displacement was 71.5 in.³ (1171.68 cm³), and the compression ratio was nominally 16:1. The engine system included an electric drive motor for both starting and running in an unfueled mode, a dynamometer, and an air ejector for removing engine exhaust gases. The fuel injection system used an American Bosch pump with a manual timing advance unit, and the fuel injection nozzle had four 0.0138-in. (0.35/-mm)-diam. spray holes arranged symmetrically on a conical surface with a 145-deg included angle. A photograph of the TACOM engine is shown in Fig. 3.

The engine timing cycle is shown in Fig. 4, and the valve and fuel injection timing is shown in Table I. The two fuels used for these experiments were n-heptane (C₇H₁₆) and diesel no. 2.

The ratio (r'/ℓ') of the crank radius and connecting rod length for the TACOM engine was 0.25, and the clearance volume V_o of the engine was 78.74 cc, as provided by the engine parameters and Eq. (2). Therefore, Eq. (6) can be evaluated to give the volume - crank angle relation

$$V(\theta), \text{cc} = 78.74 \left\{ 1 + 7.44 \left[(1-\cos \theta) + \left(\frac{1}{16} \right) (1-\cos 2\theta) \right] \right\} \quad (7)$$

The linear clearance s_o can be obtained using the relation

$$s_o = \frac{V_o}{A} = \frac{\bar{D}}{A(r-1)} \quad (8)$$

which yields the result

$$s_o \approx 0.8 \text{ cm}$$

Because only 0.8 cm clearance existed within the windowless cylinder head for the injection of the laser beam and the observation of the scattered radiation, it was necessary to modify both the piston crown and the cylinder head assembly. To provide optical access to the combustion cylinder, a spacer plate was installed between the cylinder barrel and head. A dimensioned drawing of this spacer is shown in Fig. 5.

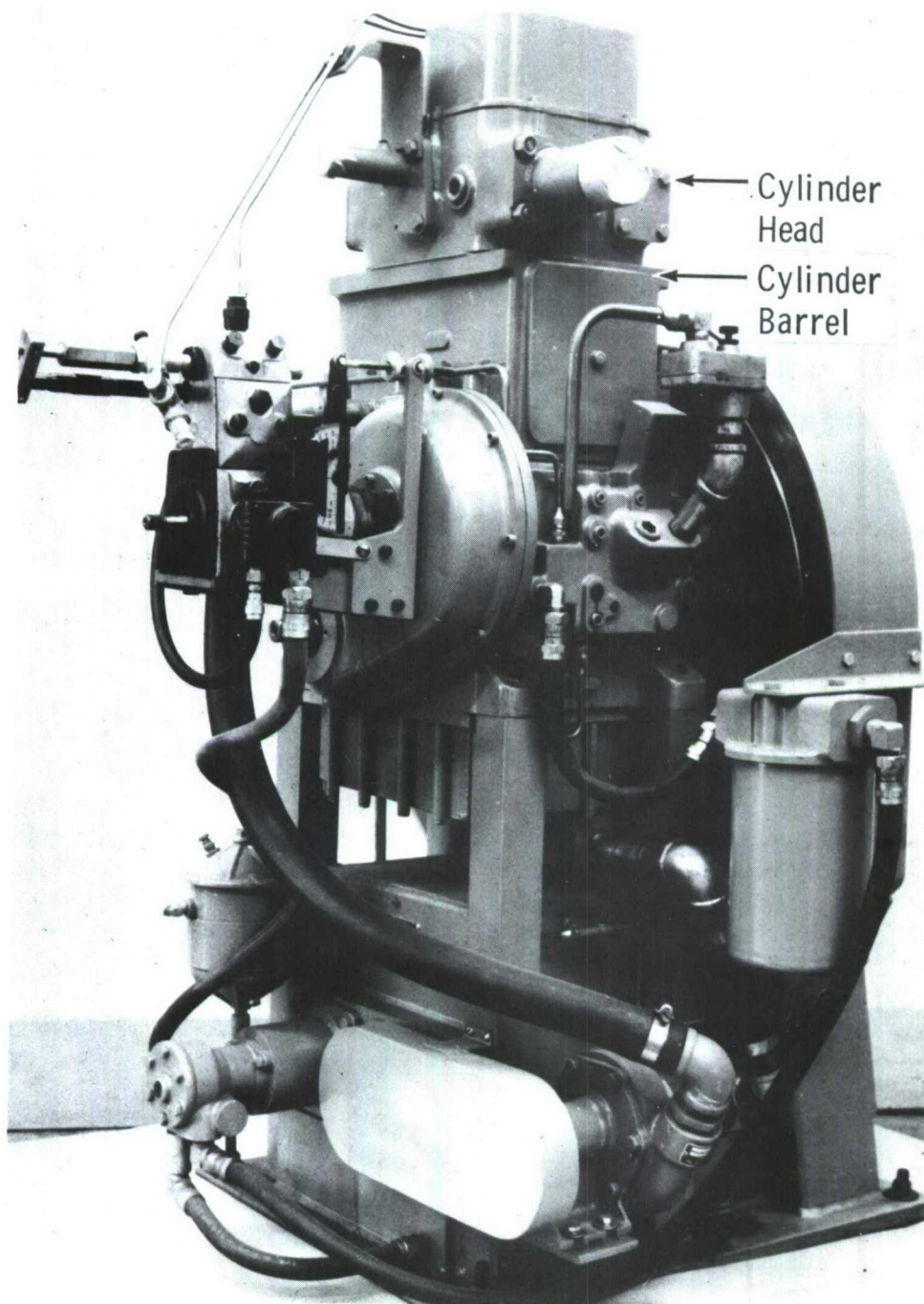


Figure 3. Photograph of TACOM engine.

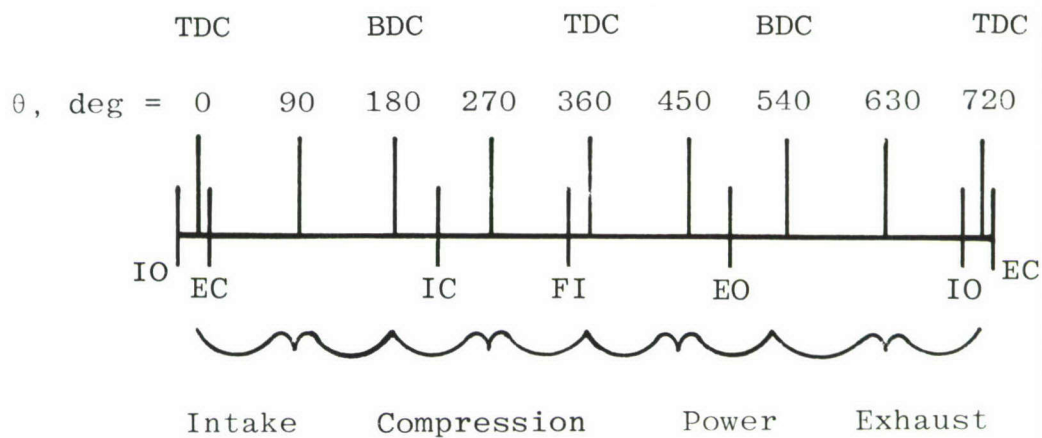
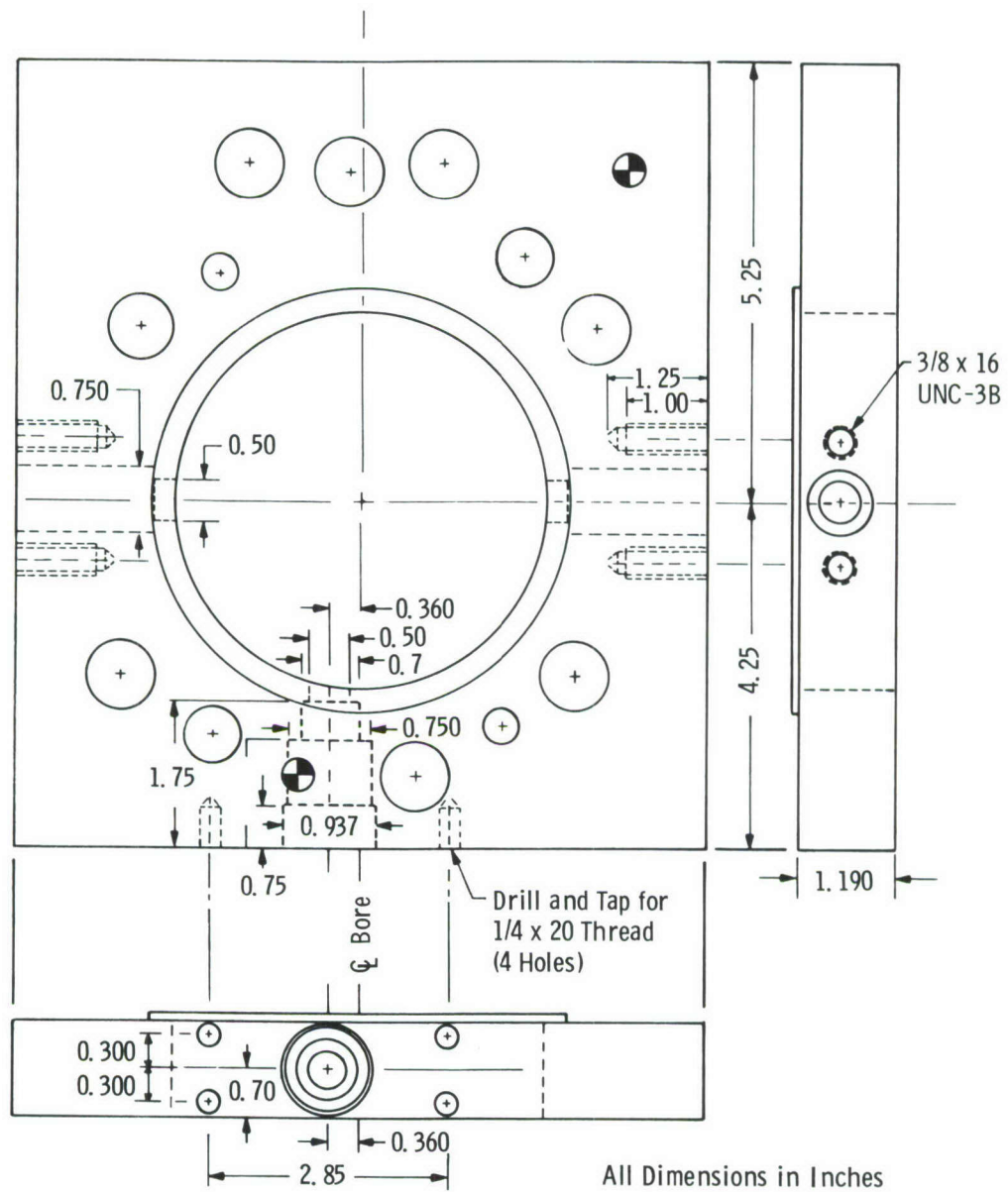


Figure 4. Engine timing cycle.

Table 1. Valve/Fuel Injection Timing	
Operation	θ , deg
Intake Opens (IO)	700°
Exhaust Closes (EC)	10°
Intake Closes (IC)	220°
Fuel Injection (FI)	340°
Exhaust Opens (EO)	490°



Optics ports were located in the spacer for the installation of 0.745-in. (18.92 mm) diam, 0.5-in. (12.7 mm)-thick quartz windows. The locations of the ports were dictated by the cooling passages and the headbolt pattern.

To compensate for the volume added by this spacer, a piston crown extension was fabricated. Modifications to the crown were also required to allow measurements throughout the entire combustion cycle. Slots were machined across the piston crown to allow passage of the laser beam across the combustion chamber, and a groove was machined perpendicular to the laser channel for passage of scattered radiation. To compensate for the optical slots, the crown dish depth was decreased. A dimensioned drawing of the modified piston is shown in Fig. 6. Computations and compression measurements indicated that the modifications resulted in a 3.4 percent decrease in V_o , or a 0.21 percent decrease in V_{max} .

An effort was made to minimize the added reciprocating mass attributable to the modified piston crown, because engine vibration could be a serious optical misalignment problem. Mass was machined from underneath the piston crown and the top of the connecting rod, and the diameter of the hole through the piston pin was increased from 0.7 in. (17.8 mm) to 1.25 in. (31.8 mm). To further minimize vibration effects, approximately 1,000 pounds of scrap iron were attached to the engine head, and vibrational displacements were restricted to less than 0.3 mm for an engine speed of 1,000 rpm.

2.2 LASER SYSTEM

A schematic drawing of the experimental setup is shown in Fig. 7, and the laser system is shown attached to a specially fabricated optical bench that was securely mounted to the top of an aluminum table. The optical bench provided micrometer adjustment of the horizontal and vertical position of the laser beam within the combustion chamber of the engine. The basic laser system was a Holobeam 620 series pulsed ruby that could be operated in either the Q-switch or conventional mode. The ruby rod was 6-in. (15.2 cm) long and 3/8-in. (0.953 cm) in diameter. A Pockels cell provided the Q-switching mechanism, and for conventional mode operation a near-totally reflecting mirror was placed between the rear of the laser and the Pockels cell.

In the conventional mode of operation the laser beam was expanded in diameter by a factor of 3, and a 500-mm focal length lens was used to focus the beam at a selected point within the combustion chamber. No beam expansion for Q-switch operation was used.

Following traversal of the combustion chamber, the laser beam energy was measured with a pyroelectric detector. A second laser energy monitor was installed at the rear of the

Pockels cell. A portion of the very weak beam transmitted by the rear mirror of the laser cavity was split off, passed through laser line filters, and detected by a photomultiplier tube. Integration of the photomultiplier output pulse gave a measure of the laser output energy, which had a maximum of 3.5 Joules.

In the Q-switch mode of operation, laser output was available at both the fundamental and second harmonic wavelengths. The 3471.5 Å wavelength was achieved by frequency doubling of the 6943 Å output radiation, using a 45-deg Z-cut, temperature-tuned, rubidium dihydrogen arsenate (RDA) crystal. The beam diameter from the laser was reduced to a nominal 7 mm with an iris diaphragm before the beam entered the crystal. The energy of the beam entering the crystal was limited to 1.5 Joules to prevent damage to the crystal. A copper sulfate solution filter at the exit of the crystal cell removed the 6943 Å primary beam and passed the 3471.5 Å beam with little attenuation. The temperature-controlled, sealed crystal cell was enclosed in a Micarta® jacket and mounted in an optical positioning device which provided transverse, vertical, pitch, yaw, and rotational adjustment of the crystal. When the cell was properly positioned and temperature-tuned, as much as 450 millijoules of 3471.5 Å radiation could be directed into the engine.

To facilitate alignment of the ruby laser system, a helium-neon (He-Ne) laser was installed behind the rear laser energy monitor. The He-Ne laser was initially aligned/auto-collimated through the center of all the ruby laser optics in use to keep the center of the ruby laser beam coincident with that of the He-Ne beam. Any necessary adjustments or periodic checks on system alignment could be made with the He-Ne beam.

2.3 SPECTROMETER SYSTEM

As shown in Fig. 7, the spectrometer was mounted on an aluminum table. Raman scattered radiation was collected from an observation volume in the combustion chamber by a 4-in.(10.2 cm)-diam. quartz lens. The object distance was 17 in. (43.2 cm), and the image distance to the spectrometer entrance slit was 25.5 in. (64.8), giving a magnification factor of 1.5. A pair of mirrors was used to rotate the image of the observed region to align the length of the focal volume along the length of the spectrometer entrance slit. The observation volumes for conventional and Q-switch laser operations were 5 mm³ and 2 mm³, respectively.

A special housing was installed in front of the spectrometer entrance slit to hold filters and/or Polaroid® sheets. Schott® filters RGN9 and GG-385 were used to block Rayleigh/Mie scattered radiation at 6943 Å and 3471.5 Å, respectively, from entering the spectrometer when vibration-rotation band measurements were made. HN22 Polaroid sheet was used to help block unpolarized particulate incandescence when the laser wavelength was 6943 Å.

The spectrometer used for spectral dispersion was a 0.85-m Spex® double spectrometer with 1200g/mm gratings blazed at 5000 Å and a nominal reciprocal linear dispersion of 4.5 Å/mm. Either the normal single exit slit was used, or it was replaced with a fixed-width (2 mm) double slit assembly (Ref. 19).

Detection of the Raman scattered radiation was achieved with cooled (-26°C) RCA-C31034A photomultipliers. Coupling to the double slits was achieved with a combination of mirrors, wedge prisms, and lenses; coupling to the single slit required only a lens.

2.4 DATA ACQUISITION SYSTEM

A different data acquisition method was employed during these experiments for each of the modes of laser operation — conventional or Q-switch. The basic technique was to integrate the photomultiplier tube (PMT) outputs during the period of peak laser output; this technique was applicable to either mode of laser operation, provided that the speed of the integration device was compatible with the experiment.

The method for conventional mode operation was to use the photon counting technique. PMT signals were processed by Ortec® Model 454 amplifiers, Model 436 discriminators, and Model 774 counters. Photon counts were obtained immediately before laser output for a background measurement and at the peak of laser output for the data measurement. Both counting intervals were 60 μsec , which corresponded to 0.36 crank angle degrees (CAD) at an engine speed of 1,000 rpm.

The data acquisition method for Q-switch mode operation was to integrate the output pulse from the photomultiplier with a LeCroy® Model 2250L fast integrator. The integrator was gated on during the output pulse of the photomultiplier to obtain a data measurement and 15 μsec after the pulse to obtain a background measurement. These integration intervals were both 200-nsec wide.

A microprocessor system was used for both modes of laser operation to control data acquisition and to record the data. The microprocessor was synchronized with the engine crank angle position and the firing of the laser, and data were acquired at appropriate times during a preset number of data cycles. The data were then printed on a teletype (TTY) for permanent record.

System timing for both operational modes was based on the crank angle sensor and comparator. At a preselected angle in the crankshaft rotation, the comparator gave a reference pulse which triggered timing and delay circuits for controlling the data acquisition system.

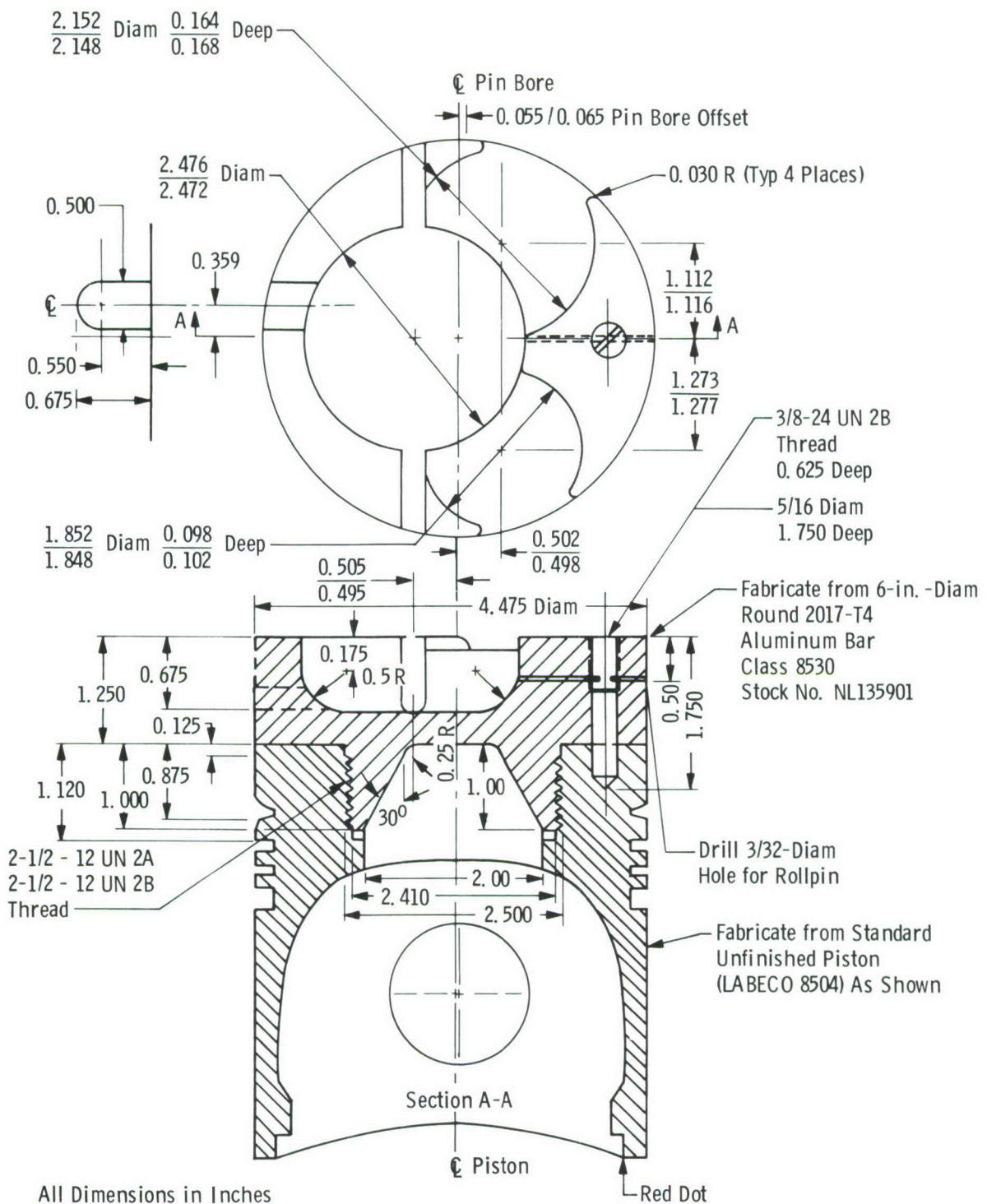


Figure 6. TACOM engine modified piston.

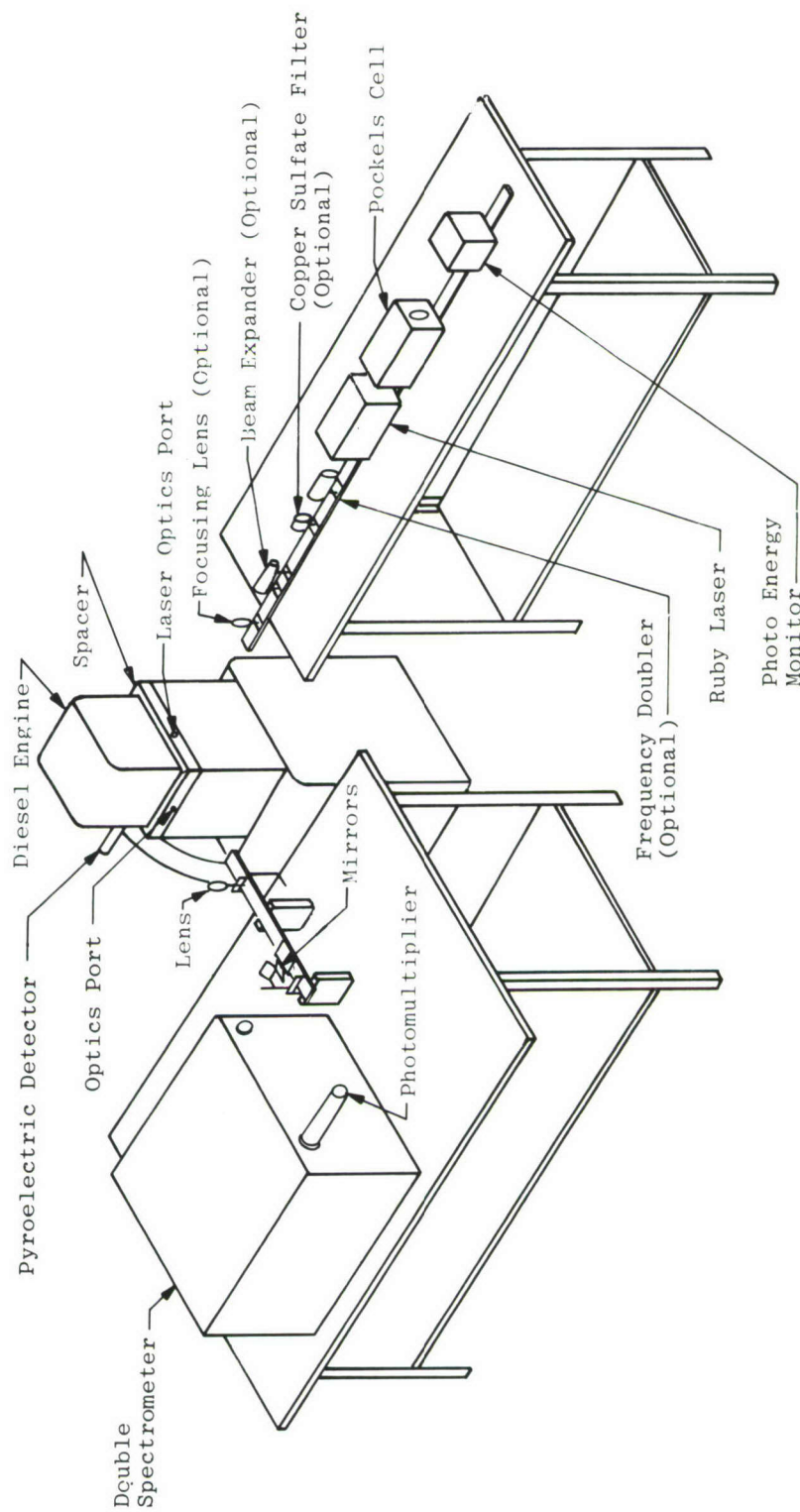


Figure 7. Diesel engine experimental setup.

Figure 8 is a block diagram of the conventional mode data acquisition system. The microprocessor initiated data acquisition with the laser charge command and synchronized the timing of the system by monitoring the 500-msec interval pulse. Data counting intervals were initiated and controlled by timing circuits which were triggered upon laser firing. Upon reaching a preset charge level, the laser was fired on coincidence of the crank angle pulse and a delayed sweep generated by the oscilloscope.

Figure 9 shows the timing diagram for the conventional mode data acquisition sequence. The timing sequence was triggered by the crank angle pulse of the delayed sweep of the oscilloscope. The duration of the sweep was such that the next crank angle pulse was skipped, and the sweep was terminated 1 msec before the succeeding pulse. If the laser was charged to its proper level, the third pulse fired the laser which, in turn, triggered the background gate, the interval pulse, and the O/S delay (shown in Fig. 7). The background gate enabled a background radiation measurement, and the O/S 2 delay provided separation between the background and data gates. The O/S 2 delay was timed so that the data gates occurred at the peak of laser output. The end of the data cycle was marked by the end of the interval pulse. The number of repetitions of this cycle was determined by a number preset in the microprocessor by means of TTY input before data acquisition.

Figure 10 is a block diagram of the Q-switch mode data acquisition system. As in the conventional mode operation, the microprocessor initiated laser charge and was synchronized with the system by monitoring the interval pulse. The laser charged to a preset level and fired on coincidence of the crank angle pulse and the PMT gate. The PMT pulse was integrated, and a background measurement was also made. The resultant data were stored in the internal memory of the integrator. At each interval, the microprocessor read the laser energy and stored it in memory. At the end of a preset number of data cycles, the microprocessor read the data from the integrator and temporarily stored the data in its memory.

Figure 11 is a timing diagram of the Q-switch mode data acquisition sequence. The timing sequence was triggered by the crank angle pulse of the O/S 1-2 delay pulse which had a duration of 117.5 msec. The end of this pulse occurred 2.5 msec before the succeeding crank angle pulse. The trailing edge of the O/S 1-2 pulse triggered the 5-msec PMT gate which turned on the photomultiplier tube. Assuming the laser was charged, as indicated by the laser ready signal, the occurrence of the crank angle pulse fired the laser, initiated the interval pulse, and retriggered the O/S 1-2 delay. The rear laser energy monitor triggered the pulse generator which provided integrator gating. The pulse generator delayed its output until the PMT output occurred, when it produced two 200-nsec pulses separated by 15 μ sec. The first and second pulses gated the integrator for a signal and background measurement, respectively. The end of the 500-msec interval pulse marked the end of the data cycle. The PMT gate was enabled at each crank angle pulse, but it only occurred when the laser was charged.

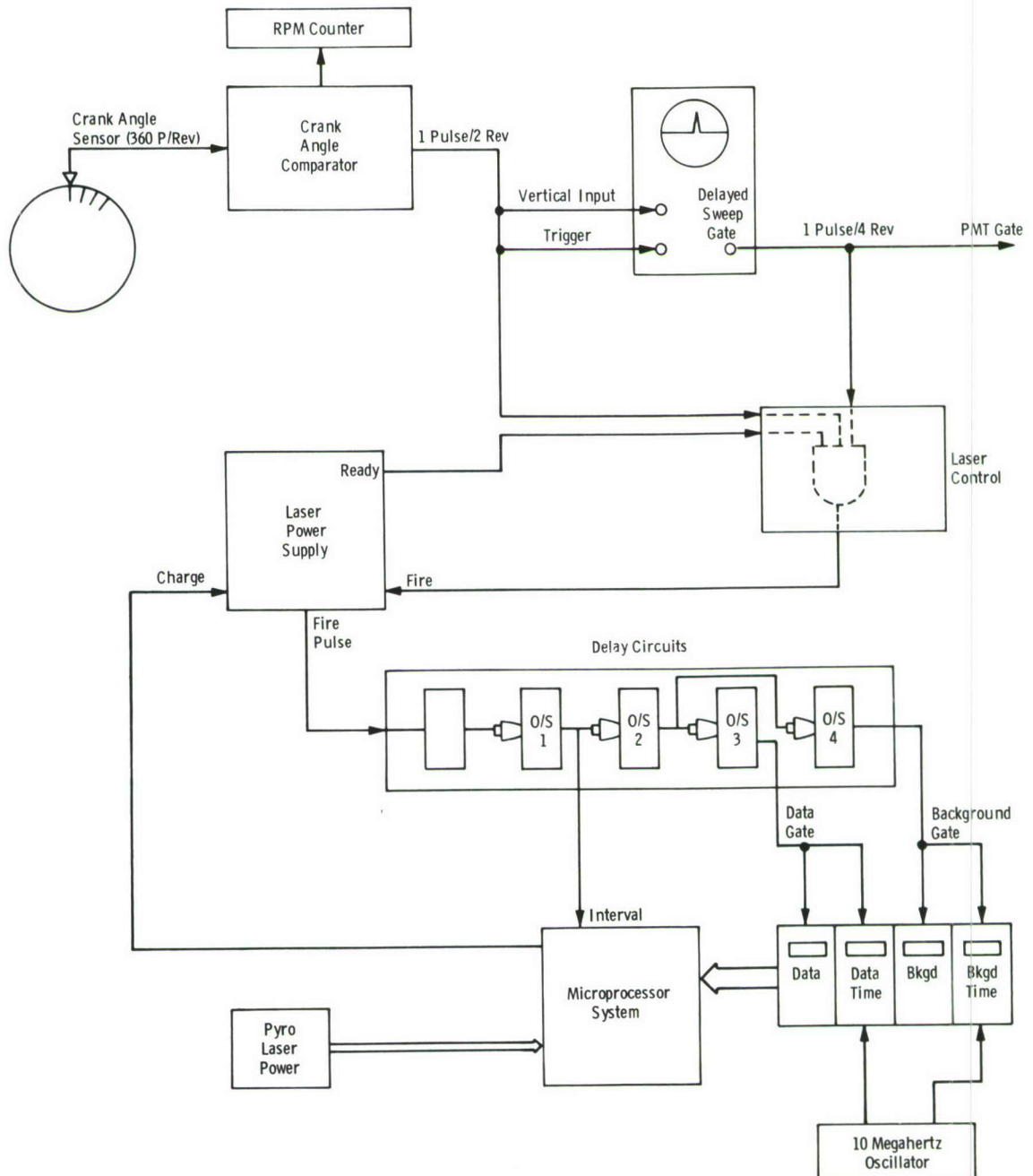


Figure 8. Block diagram of conventional mode data acquisition system.

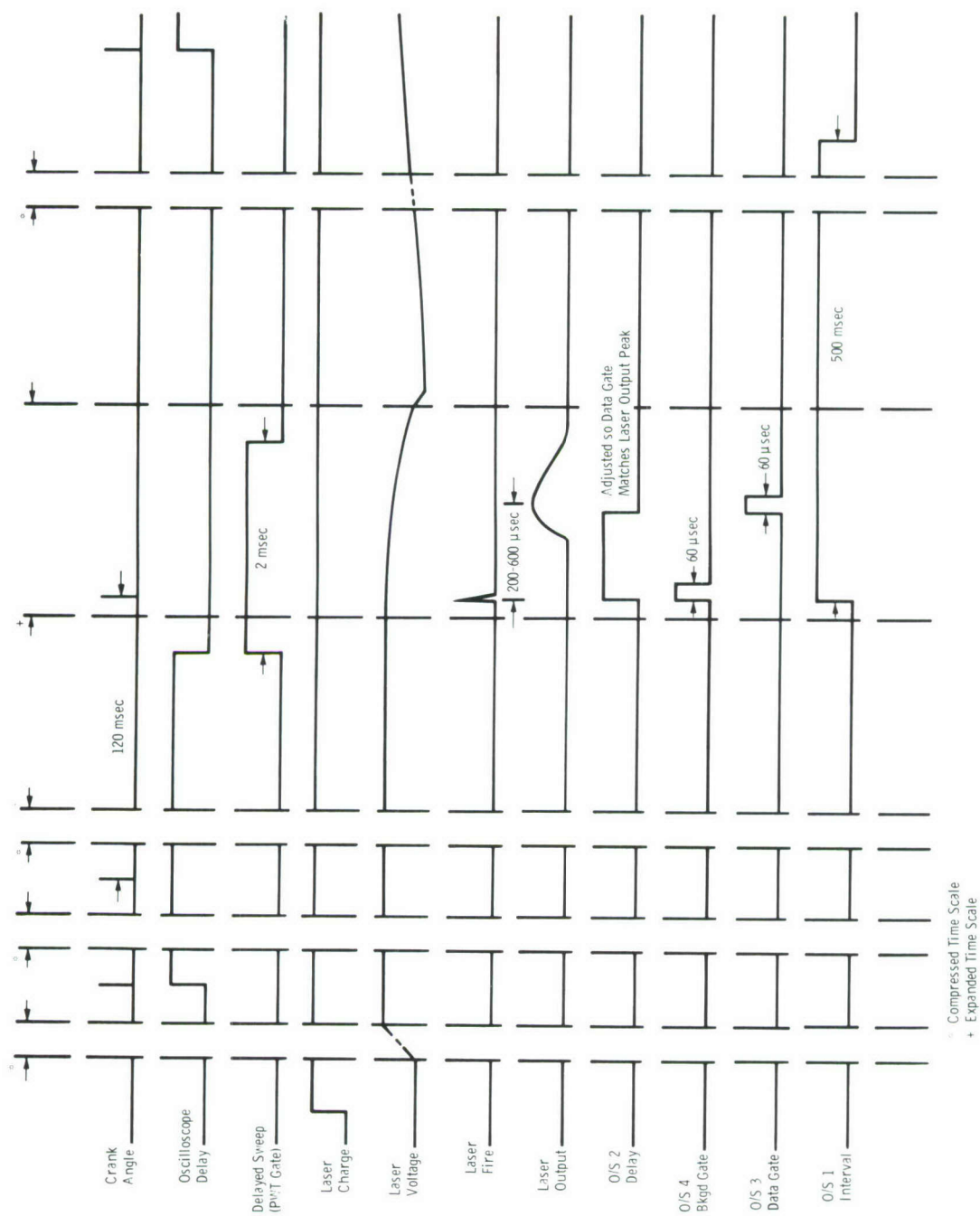


Figure 9. Timing diagram for conventional mode data acquisition system.

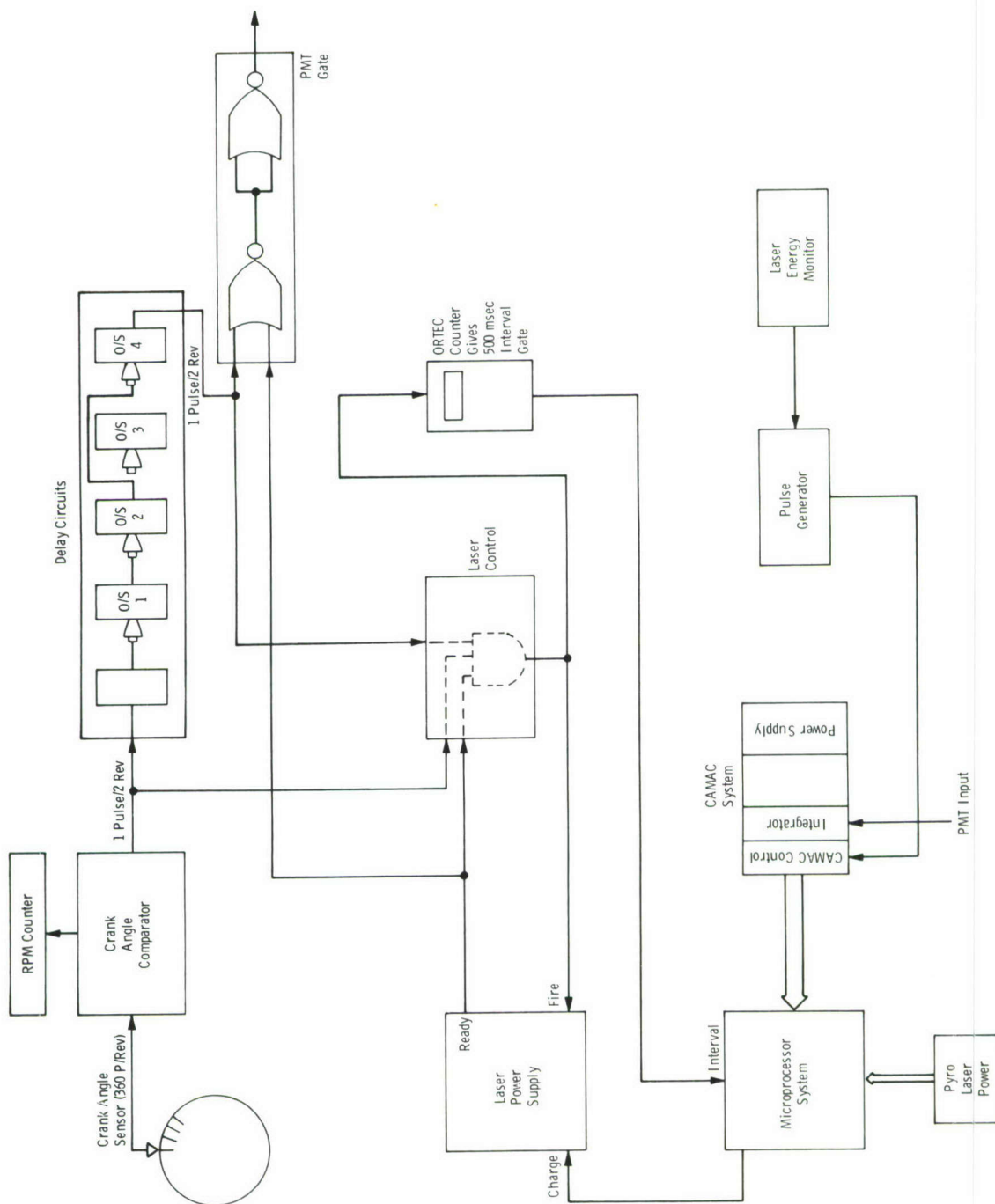


Figure 10. Block diagram of Q-switch data acquisition system.

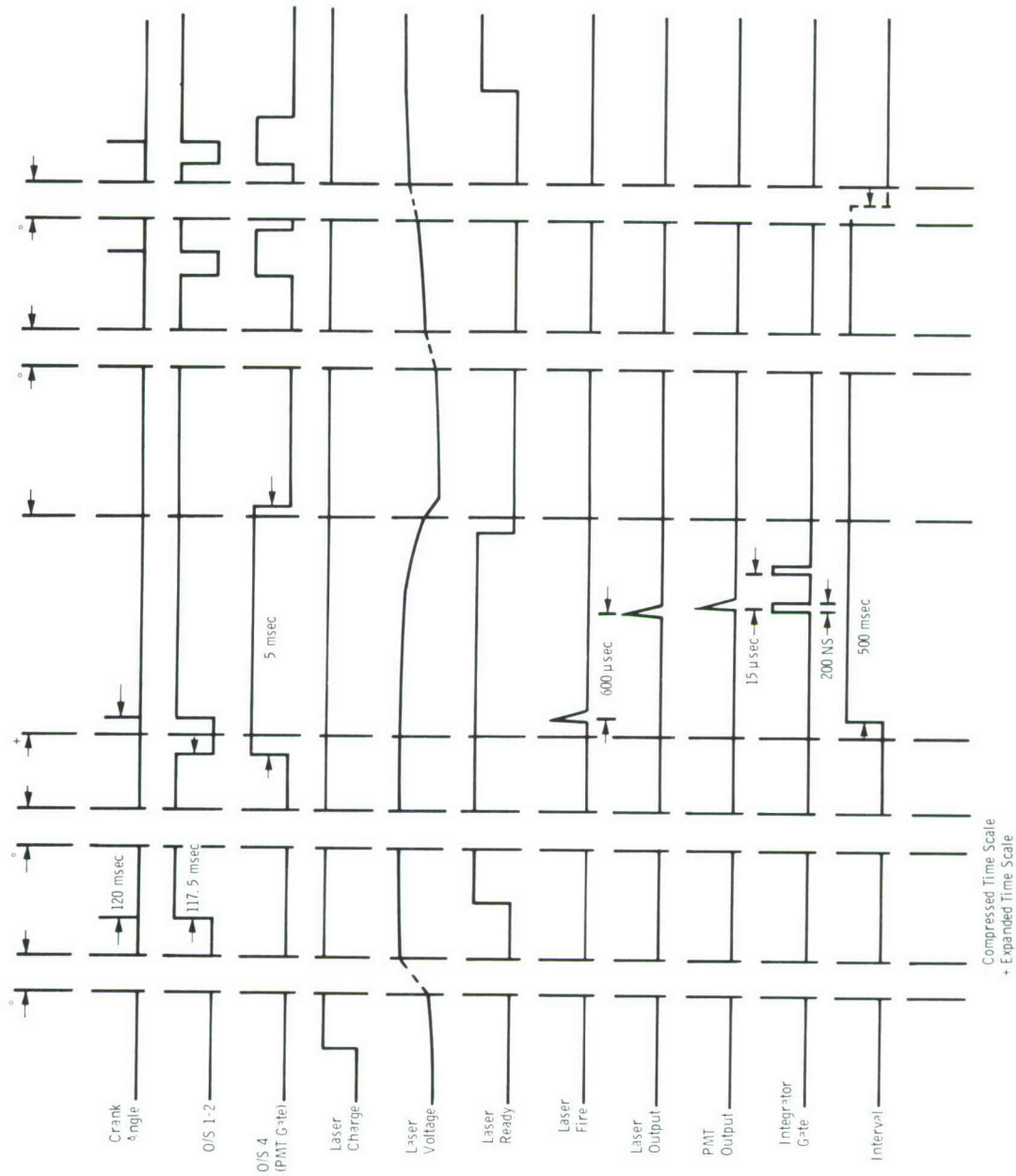


Figure 11. Timing diagram of Q-switch data acquisition system.

3.0 LASER-RAMAN MEASUREMENT TECHNIQUE

3.1 VIBRATIONAL RELAXATION CONSIDERATIONS

It has been asserted previously that Raman scattering is capable of determining local, time-resolved measurements of the gas temperature. More precisely, Raman scattering, like the majority of other optical diagnostic techniques, determines the temperatures or energy distributions of the internal molecular mode of motion which is interrogated by the scattering or absorption process. In the case of spontaneous Raman scattering as used in this work, the temperatures T_R and T_V of the vibrational and rotational modes, respectively, of the ground electronic state of N_2 are measured. Consequently, only if the rotational and vibrational modes are in local thermal equilibrium with the translational mode of N_2 does the Raman scattering measurement of T_R and T_V yield the local gas, or translational, temperature (T_{tr}).

As will be discussed in a later section, it was desirable to use vibrational Raman scattering to determine T_V and from T_V , infer T_{tr} for the fueled mode operation of the engine. Therefore, it was necessary to ensure that the vibrational mode remained in sensible equilibrium with the translational mode. Since the N_2 vibrational mode for the temperature range of this study can be described adequately by a simple harmonic oscillator, the vibration-translation energy transfer mechanism can be characterized by a single relaxation time (τ_v). A relevant characteristic time (τ) for the engine is $1/\omega$, where ω is the angular speed of revolution of the engine. For order of magnitude purposes, if T_V is to be essentially equal to T_{tr} ,

$$\tau_v \ll \tau$$

or

$$\omega \tau_v \ll 1 \tag{9}$$

For operation of the engine at 1,000 rpm:

$$\tau_v \ll 10^{-2} \text{ sec}$$

In terms of Z_{10} , the number of intermolecular collisions required for vibrational deexcitation, and Z_c , the intermolecular elastic collision rate, the vibrational relaxation time for a pure gas can be written as

$$\tau_v = Z_{10}/Z_c \tag{10}$$

Using the data of Cottrell and McCoubrey (Ref. 20), Z_{10} was found to be represented adequately by

$$\log Z_{10} = 8.866 - 2.527 \times 10^{-3} T \quad (11)$$

Further, representing the intermolecular interaction by the Lennard-Jones 12:6 potential,

$$Z_c = 2 n \sigma^2 \Omega^{(2,2)*} [\pi R T / M]^{1/2} \quad (12)$$

where

M = gram molecular weight

n = number density

R = universal gas constant

σ = potential range parameter of the
Lennard-Jones potential (Ref. 21)

and

$\Omega^{(2,2)*}$ = collision integral (Ref. 21).

Evaluation of Eq.(10) for N_2 at $T = 400$ K and $n(N_2) = 10^{13} \text{ cc}^{-1}$ gives $\tau_v(N_2) \approx 5 \times 10^{-2} \text{ sec}$ which does not satisfy Eq. (9). Therefore, for low temperatures for $n \leq 10^{20} \text{ cc}^{-1}$, significant vibrational relaxation and differences between T_v and T_{tr} may exist. As T increases to 1000 K, τ_v decreases such that $\tau_v \approx 10^{-3} \text{ sec} \ll 10^{-2} \text{ sec}$.

Considering initially the unfueled mode of operation of the engine and the implications of these results, the peak value of the temperature of the assumed-adiabatic process is 906 K for a compression ratio of 15.88. Consequently, if N_2 were the working gas, the magnitude and variation of τ_v are such that near-equilibrium is to be expected near top dead center (TDC) and vibrational lag is to be anticipated for the lower temperature portions of the cycle. To demonstrate this effect, the time (t)-dependent, vibrational relaxation equation

$$dE_v/dt = -\frac{1}{\tau_v} (E_v - E_{ve}) \quad (13)$$

for the vibrational energy, E_v , was solved for N_2 subjected to an adiabatic, periodic variation in density and temperature. In Eq. (13) E_{ve} is the equilibrium value of E_v .

For this calculation it was assumed that the gas density varied inversely with the volume, as given by Eq. (3) and that the vibrational mode enthalpy was sufficiently small to preclude any effect of the relaxation process on the translational mode properties. Further, the

specific heat ratio was assumed to be 1.40. Figure 12 shows the calculated values of T_v and T_{tr} as a function of crank angle, θ , for an engine speed of 1,000 rpm. Significant relaxation for N_2 can be expected for all regions of the cycle except in the vicinity of the compression peak, a result which is consistent with the order of magnitude estimates.

If the working gas is air rather than N_2 , O_2 decreases τ_v of N_2 and enhances equilibration. Similar conclusions are applicable to other, but minor, species such as H_2O and CO_2 . If $\tau_{v,i}(N_2)$ denotes the relaxation time appropriate to the deactivation of a single N_2 molecule in a heat bath of A-species and X_A denotes the mole fraction of A-species in the gas mixture, the mixture relaxation time $\tau_{v,mix}(N_2)$ is given by (Ref. 20):

$$\frac{1}{\tau_{v,mix}(N_2)} = \sum_i X_i / \tau_{v,i} \quad (14)$$

The effect of O_2 and the minor impurities of air is to decrease $\tau_v(N_2)$ by an order of magnitude (Ref. 20). Consequently, only for the very low compression and temperature regions of the cycle of the unfueled engine will $T_v(N_2)$ significantly lag T_{tr} .

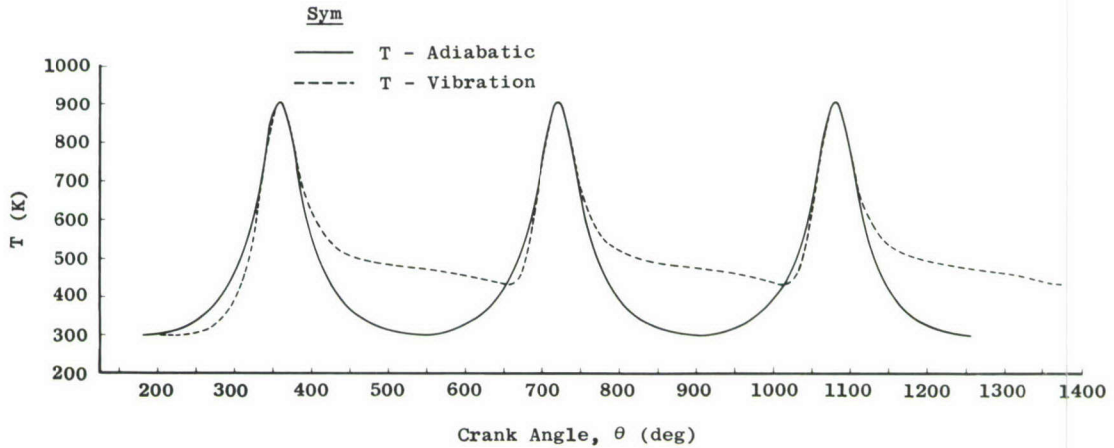


Figure 12. Vibrational relaxation as a function of crank angle.

For the fueled mode of operation, similar conclusions apply before combustion and the presence of additional impurities will tend to speed the equilibration process. Upon combination, the gas temperature increase may be sufficiently rapid that significant departures of T_{tr} from $T_v(N_2)$ might occur. To evaluate the likelihood of this occurrence, it is assumed that T_{tr} increases step-wise from 1000 K to 2000 K. The evaluation of Eq. (10) at $T_{tr} = 2000$ K, assuming pure N_2 to be the working gas, shows that the lag in T_v relative to T_{tr} is on the order of 0.1 CAD, which is insignificant for this study. Again, the effects of impurities can be expected to decrease this already insignificant vibrational lag.

Therefore, these calculations show that the use of vibrational Raman scattering and the measurement of T_v of N_2 can be expected to provide an excellent measure of T of the gas for either the fueled or unfueled operation of the engine for all regions of the cycle, except those corresponding to the low compression-temperature regions.

3.2 SPECTRA AND INTENSITY RELATIONS

The temperature dependence of the spectrometer-convolved intensity distribution of Raman lines of various molecular species can be readily calculated with the Raman Spectral Program (RASP). Figures 13 and 14 demonstrate the change in the relative intensity distribution of the Stokes vibrational-rotational band of N_2 with temperature. The relative intensities of the $v = 0$ and $v = 1$ Q-branches (noted in Figs. 13 and 14) are functions of temperature and, using RASP, the ratio of the intensities,

$$R_v = I_c(N_2, Q_1) / I_c(N_2, Q_0) \quad (15)$$

can be calculated. The results of such a calculation are shown in Fig. 15; therefore, by measuring the relative intensity ratio and using the appropriate curve of Fig. 15 temperature can be determined.

The intensity of the N_2 , $v = 0$ Q-branches is directly proportional to the species number density as well as a function of temperature. This can be expressed as

$$n(N_2) = C_F(N_2) \cdot C_F(T, N_2) \cdot I_m(N_2, Q_0) \quad (16)$$

in which $n(N_2)$ is the number density, $C_F(N_2)$ is a calibration factor determined at atmospheric pressure, room temperature conditions, and $I_m(N_2, Q_0)$ is the measured intensity of the $v = 0$, Q-branch which has been normalized by the laser beam energy. The temperature-dependent correction factor, $C_F(T, N_2)$ is determined using RASP to calculate $I_m(N_2, Q_0)$ for a range of temperatures. The results of such a calculation are shown in Fig. 15.

An alternate method of temperature measurement is to use the pure rotational Raman structure as discussed in detail in Refs. 17, 19, and 22. This method was used in these experiments only for the unfueled operation of the engine, because only for the unfueled case were the gas species quantitatively known and the particulate level sufficiently low to permit adequate rejection of the Rayleigh/Mie scattered radiation. A RASP calculation of the Stokes rotational Raman spectra for air at 300 K and 1000 K is shown in Fig. 16, and the change of the band profile with temperature is readily observed. Because of the constant species mole fractions, the ratio (R_r) of the intensities of two selected portions of the band will be a function only of temperature. A comparison of measured and calculated (Fig. 17) intensity ratios will therefore determine temperature.

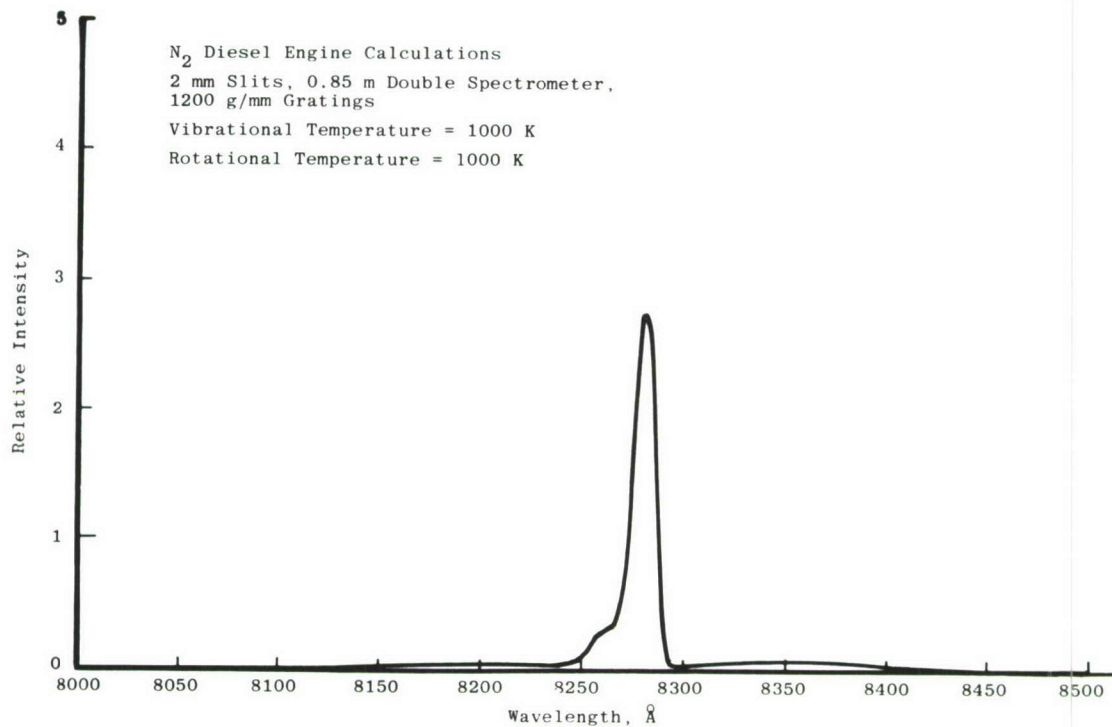


Figure 13a. N_2 VIB-ROT band, laser wavelength at 6943 Å.

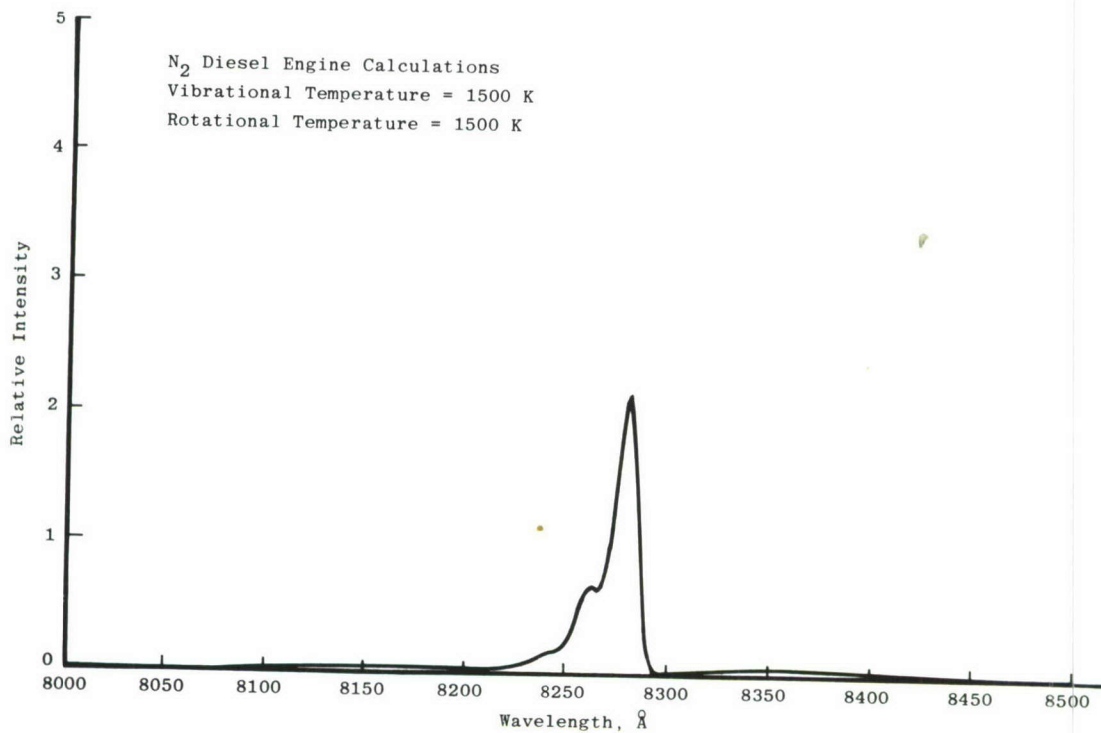


Figure 13b
 Figure 13. Concluded.

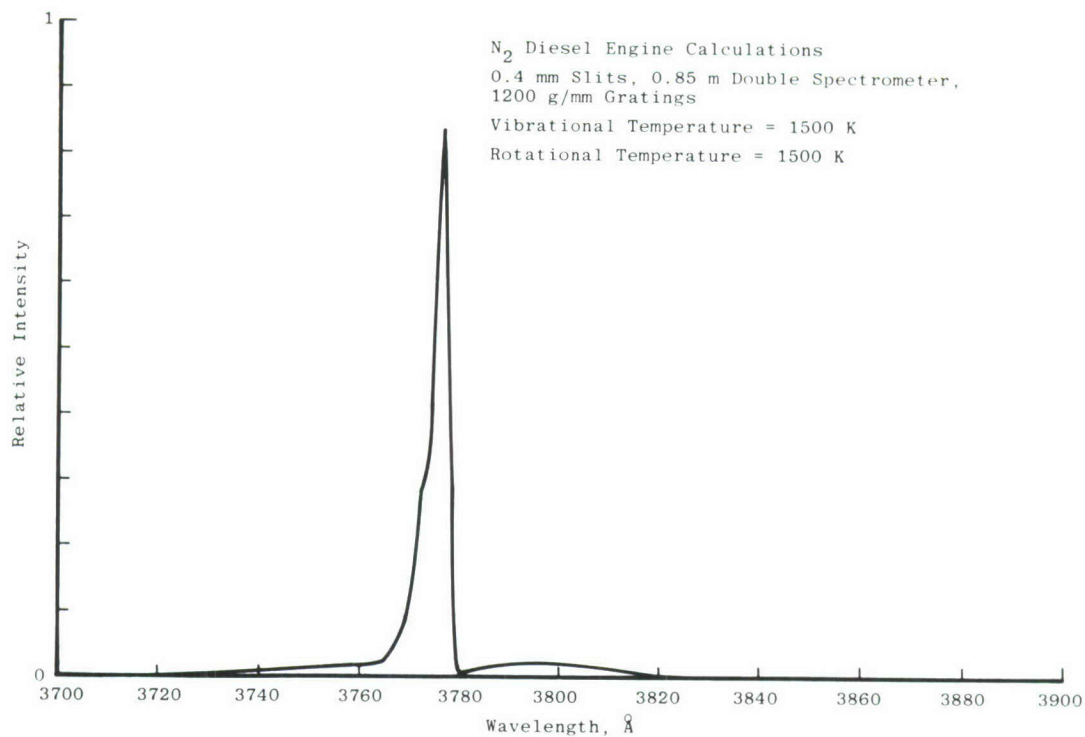


Figure 14a. N_2 VIB-ROT band, laser wavelength at 3471.5 Å.

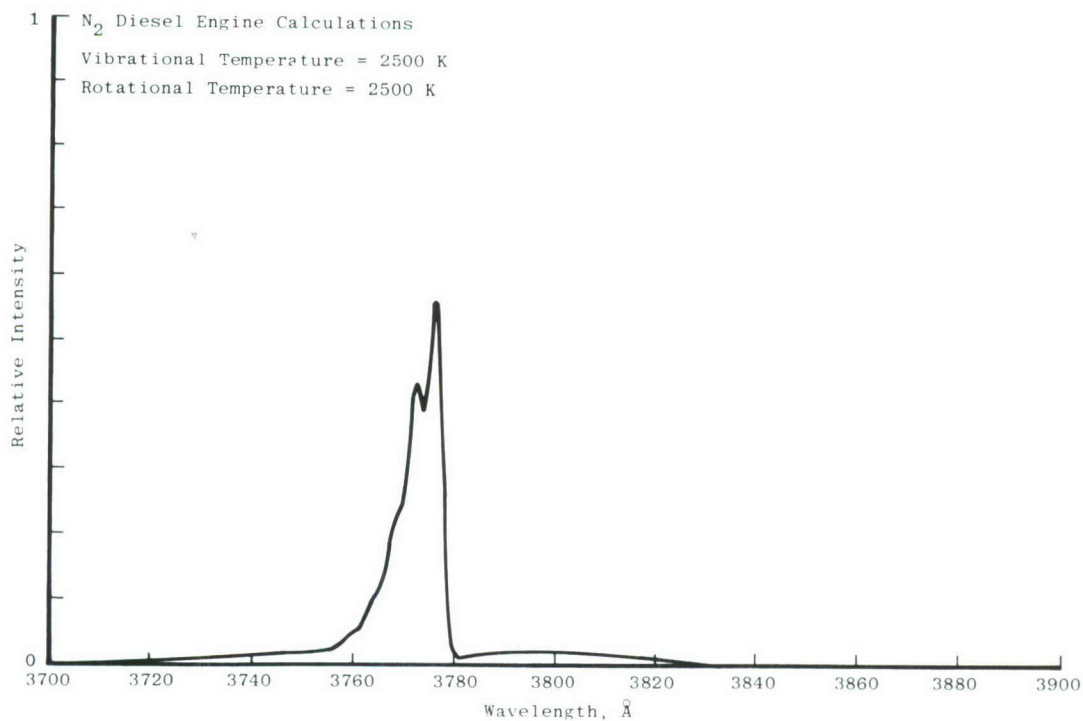


Figure 14b
Figure 14. Concluded.

3.3 CALIBRATIONS AND DATA REDUCTION

Calibrations were completed on each day that experiments were conducted with the diesel engine. The rear energy monitor and the pyroelectric detector were each calibrated as functions of the true output energy of the laser system. The calibration constant $C_F(N_2)$ was determined using measured intensity values and the dry air nitrogen number density which was calculated using measured atmospheric pressure, temperature, and relative humidity.

Whenever the double slit assembly was used, the relative sensitivity of the two detectors (R_R) was determined by adjusting the spectrometer wavelength dial to place the same Raman signal on each detector sequentially. A measured vibration-rotation band intensity ratio, for example, was determined by

$$R = \left[I_m^t(N_2, Q_1) / I_m^t(N_2, Q_o) \right] R_R \quad (17)$$

and T_v was then graphically determined from Fig. 15. A similar procedure was followed for T_R measurement.

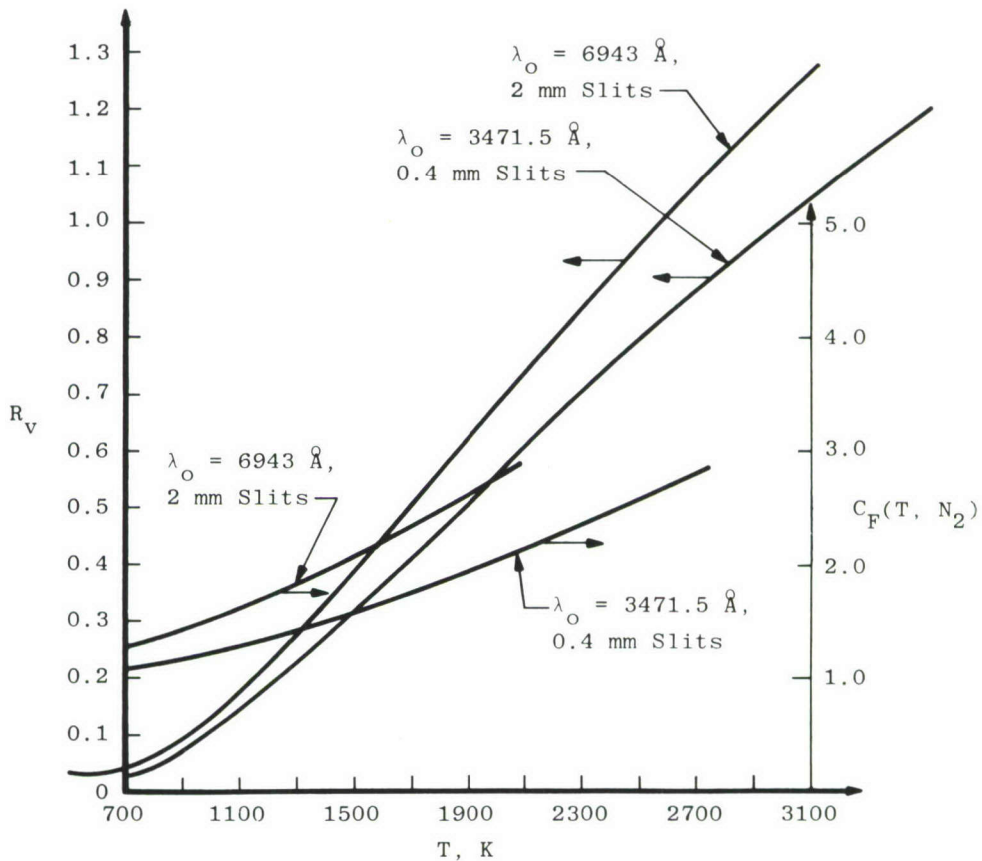


Figure 15. R_v and $C_F(T, N_2)$ as a function of temperature.

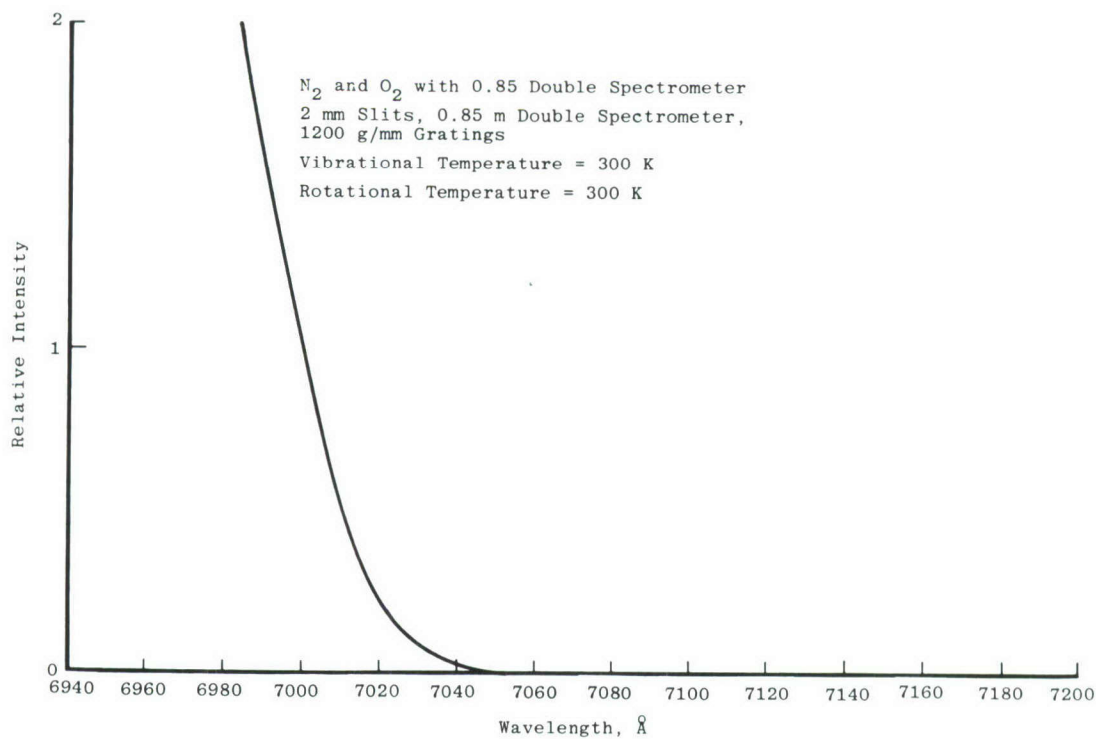


Figure 16. $N_2 + O_2$ in air Rayleigh line and pure rotational band, laser wavelength at 6943Å.

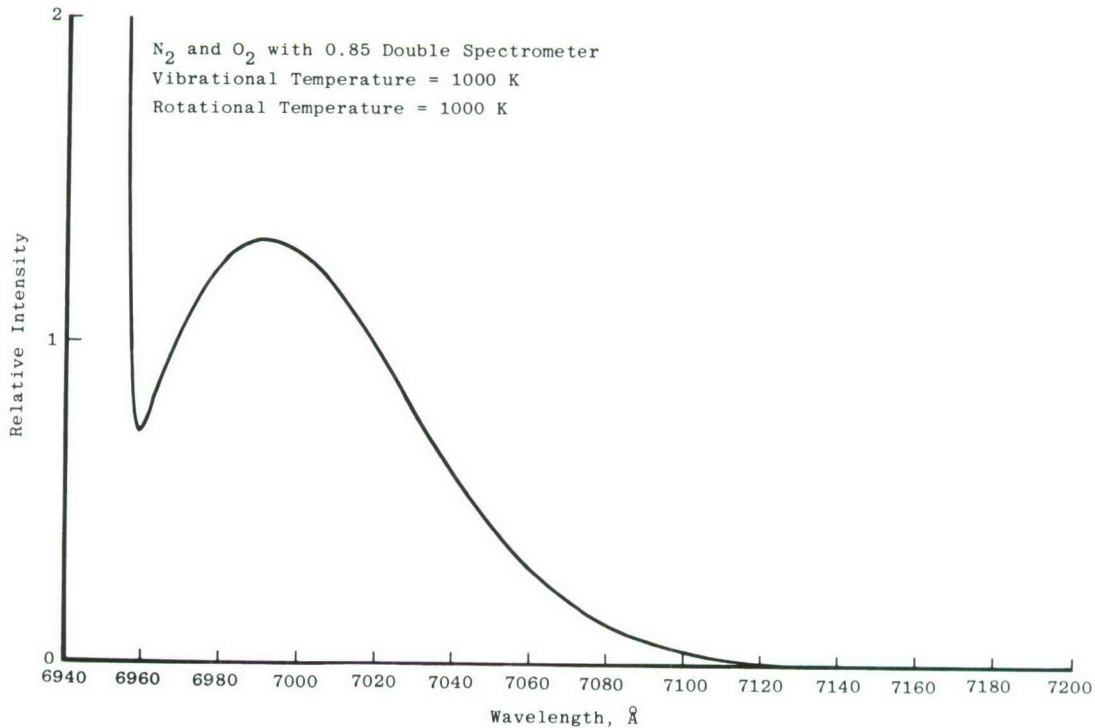


Figure 16b
 Figure 16. Concluded.

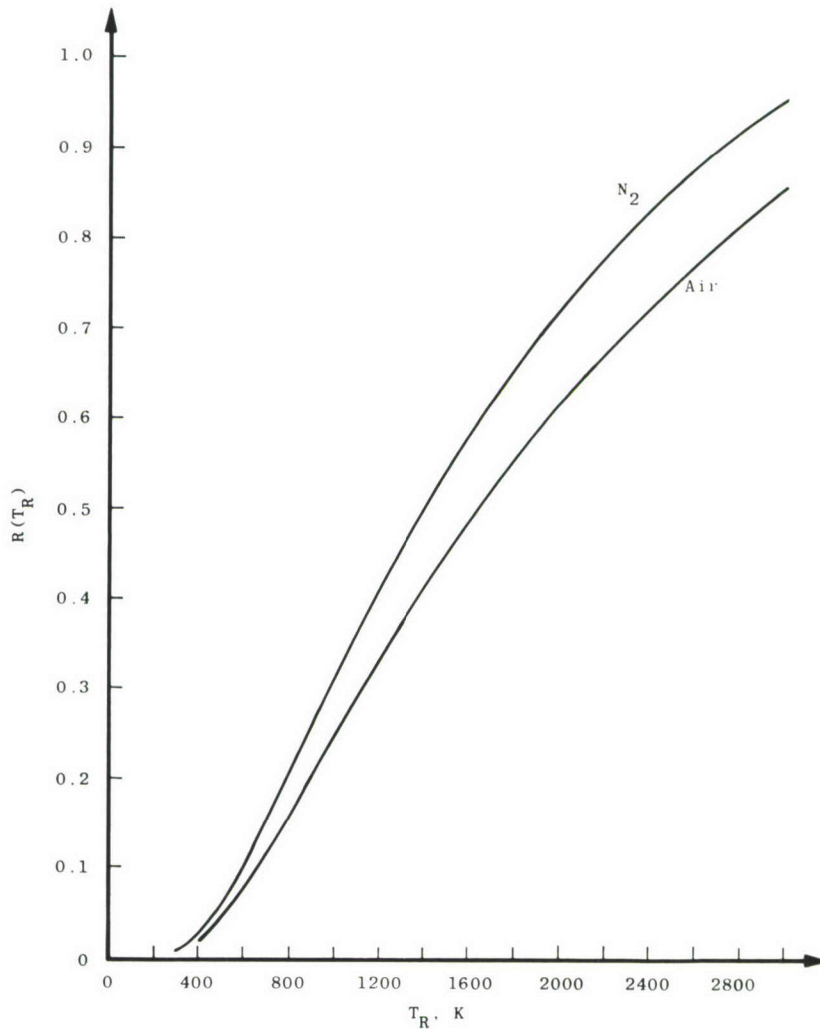


Figure 17. Intensity ratio, $I_c(7061\text{\AA})/I_c(7010\text{\AA})$, as a function of rotational temperature.

Using a measured value of T_v , a $C_F(T, N_2)$ value was graphically determined from Fig. 15, and a measured N_2 number density was then determined from Eq. (16).

Intensity values were normalized for laser energy fluctuations and transmission losses using the following relation.

$$I_m = I'_m / E_t \quad (18)$$

E_t is the estimated laser energy at the observation volume, and it is given by

$$E_t = (E_o/2) \left[(E_p/E_o)_a + (E_p/E_o) \right] \quad (19)$$

Equation (19) was assumed unreliable for the purpose of density measurement if the beam attenuation was greater than 40 percent.

On-band signals for each of the two spectral positions monitored, as well as the off-band position, were averaged over 45 laser pulses. Off-band signals were subtracted from the on-band signals to give the energy-normalized, background-corrected Raman signals which could be ratioed for a temperature measurement or used in Eq. (16) for a density measurement. As noted by Eckbreth (Ref. 23) this method gives only an "effective" average temperature, because the ratio thus formed depends on the magnitude and correlation of the number density and temperature fluctuations in the combustion chamber. Unfortunately, with the equipment that was available, on- and off-band signals could not be simultaneously recorded to permit single shot ratios (and temperatures) from being determined.

4.0 DISCUSSION

4.1 CHRONOLOGY OF EXPERIMENTS

The initial experiments were conducted using the double slit assembly and the laser in Q-switch mode at 6943 Å. Both T_R and T_V were measured for the unfueled engine, and data were acquired over ± 60 CAD with respect to TDC. The results are shown in Fig. 18; T_R and T_V are essentially equal. This was an important result, because for the fueled case it was known that use of the N_2 vibration-rotation band would be required. This was because of the large magnitude of Mie scattering from particulates which could not be sufficiently spectrally rejected in the rotational Raman regions and the spectral overlap of unknown mole fractions of N_2 , CO_2 , O_2 , H_2O , and CO in the rotational region.

For engine operation using no. 2 diesel fuel, measurements of the gas temperature were then initiated using the N_2 vibration-rotation band and the laser in Q-switch mode at 6943 Å. Several problems (some of which were anticipated) were then encountered. The combustion chamber spacer ports became very dirty after about a minute of operation unless the engine was preheated. This preheating was accomplished by bringing the engine cooling water temperature to 150°F (65.6°C) and then running the engine for approximately 10 min to bring the temperature up to 170°F (76.7°C). The optical ports were then cleaned, and approximately 5 min of engine operation could be conducted before the ports began to collect a significant amount of soot. The power density of the laser beam at the focal volume had to be maintained at less than 10^{10} watts/cm² to prevent gas breakdown caused by the heavy particulate loading in the combustion chamber. Even so, the power density needed to obtain a moderate signal-to-noise ratio in a particulate-free environment was sufficiently high to heat and partially vaporize the particulates in the combustion chamber, which

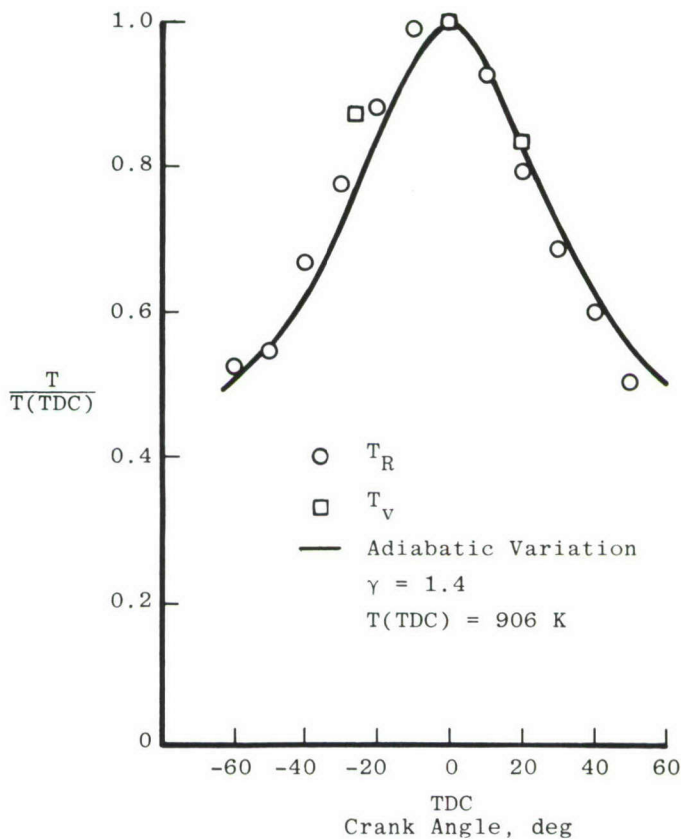


Figure 18. Variation of normalized temperature with crank angle for unfueled operation.

subsequently produced a high level of incandescent radiation with a spectrum resembling that of a blackbody. Figure 19 is a plot of the relative intensity of the laser-induced incandescence as a function of wavelength, and the blackbody radiation curve for $T = 1900 \text{ K}$ fits the experimental points very well. The laser-induced incandescence intensity also varied linearly with laser energy for a given laser setup. The high level of laser-induced incandescence was greater than the Raman signal, and the high level of background radiation from the combustion process decreased drastically the sensitivity of the photomultipliers.

At this point, n-heptane was chosen as the engine fuel for a variety of reasons: (1) n-heptane gave the appearance of unleaded gasoline and was much cleaner looking than no. 2 diesel fuel; therefore, it was anticipated that much cleaner burning might be obtained; (2) the heat of combustion of n-heptane is very similar to that of regular diesel fuel; (3) the chemical formula for n-heptane is known, and this permits direct calculation of the chemistry of the combustion process. Compared to no. 2 diesel fuel, the use of n-heptane

resulted in much lower soot accumulation on the ports for an equal engine run time, and the engine ran very smoothly. Furthermore, with n-heptane and a laser output wavelength of 6943 \AA , measurements of vibrational temperature could be made at TDC and at $\text{CAD} \geq 50$, after top dead center (ATDC), but measurements could not be made in the CAD region of 5 to 45 deg ATDC because of laser-induced incandescence.

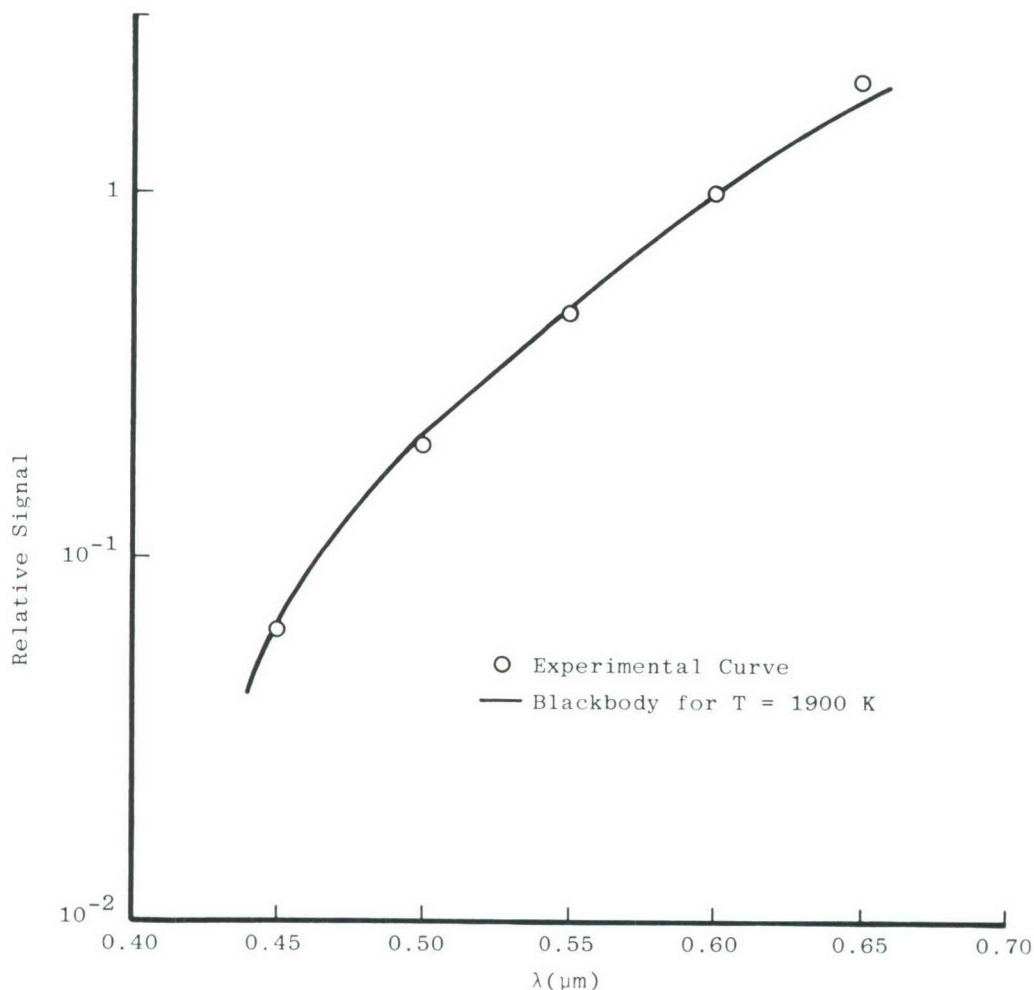


Figure 19. Comparison of laser-induced incandescence with blackbody emission.

Next, the ruby laser output frequency was doubled to 3471.5 \AA for the following reasons:

1. A signal gain of an order of magnitude was calculated as a result of optical system efficiency gain and the λ^{-4} dependence of the Raman signal.

2. A reduction in the laser-induced incandescence by a factor of 10^{-3} was calculated because the N_2 Stokes vibration-rotation band was now at 3777 \AA rather than at 8284 \AA .
3. A reduction of 10^{-3} in the background radiation from the combustion process was also anticipated, because the maximum possible temperature for the process for the fuel flow rate used was 1900 to 2200 K.

Operation with the frequency-doubled laser system did permit data acquisition throughout the combustion portion of the cycle with increased signal levels and a substantially decreased off-band laser-induced incandescence level which, because of the continuum nature of the incandescence, could be subtracted from the on-band signals. The wavelength positions for the on-band and off-band measurements are shown in Figs. 13 and 14.

4.2 RESULTS

Vibrational temperature and number density measurements obtained within the combustion chamber using n-heptane fuel are shown in Fig. 20 as functions of engine crank angle degrees for the compression/power portion of the engine cycle. Unfueled T_v measurements are also shown in Fig. 20 for reference. The fueled T_v value is only 100 K greater than the unfueled T_v value at TDC. At 20 deg ATDC the T_v has reached a maximum value of $\sim 1500 \text{ K}$; therefore, a lag of $\approx 40 \text{ CAD}$ occurs between fuel injection and the first T_v peak. After an approximate 300 K decline, T_v reaches a broad peak ranging from 45 to 80 CAD at $\sim 1650 \text{ K}$ before beginning to decline again. This unusual double-peaked temperature distribution is in qualitative agreement with H_2O and CO_2 relative species signals obtained with a mass spectrometric technique (Ref. 24) applied to the same engine but for no. 2 diesel fuel. Furthermore, a qualitatively similar temperature profile was measured in Ref. 23 using the infrared emission from the engine at $3.35 \text{ }\mu\text{m}$.

Considering the continuous degradation of the port transmission values during a data acquisition sequence, the agreement between measured and calculated density values is gratifying. Additionally, the agreement between the measured and experimental values of N_2 number density in the CAD range of 50 to 90 deg is particularly encouraging for two reasons: (1) the N_2 number density was expected to agree closely with the prediction at this late stage of the combustion; (2) large temperature correction factors $C_F(T, N_2)$ had to be used to obtain $n(N_2)$ values. This agreement supports the reliability of the measured temperature values in that CAD range. Absolute N_2 number densities were not possible in the 0 to 45 deg CAD range because of large attenuation of the laser beam intensity (50 to 90 percent) and the consequent ignorance of its precise value at the scattering volume.

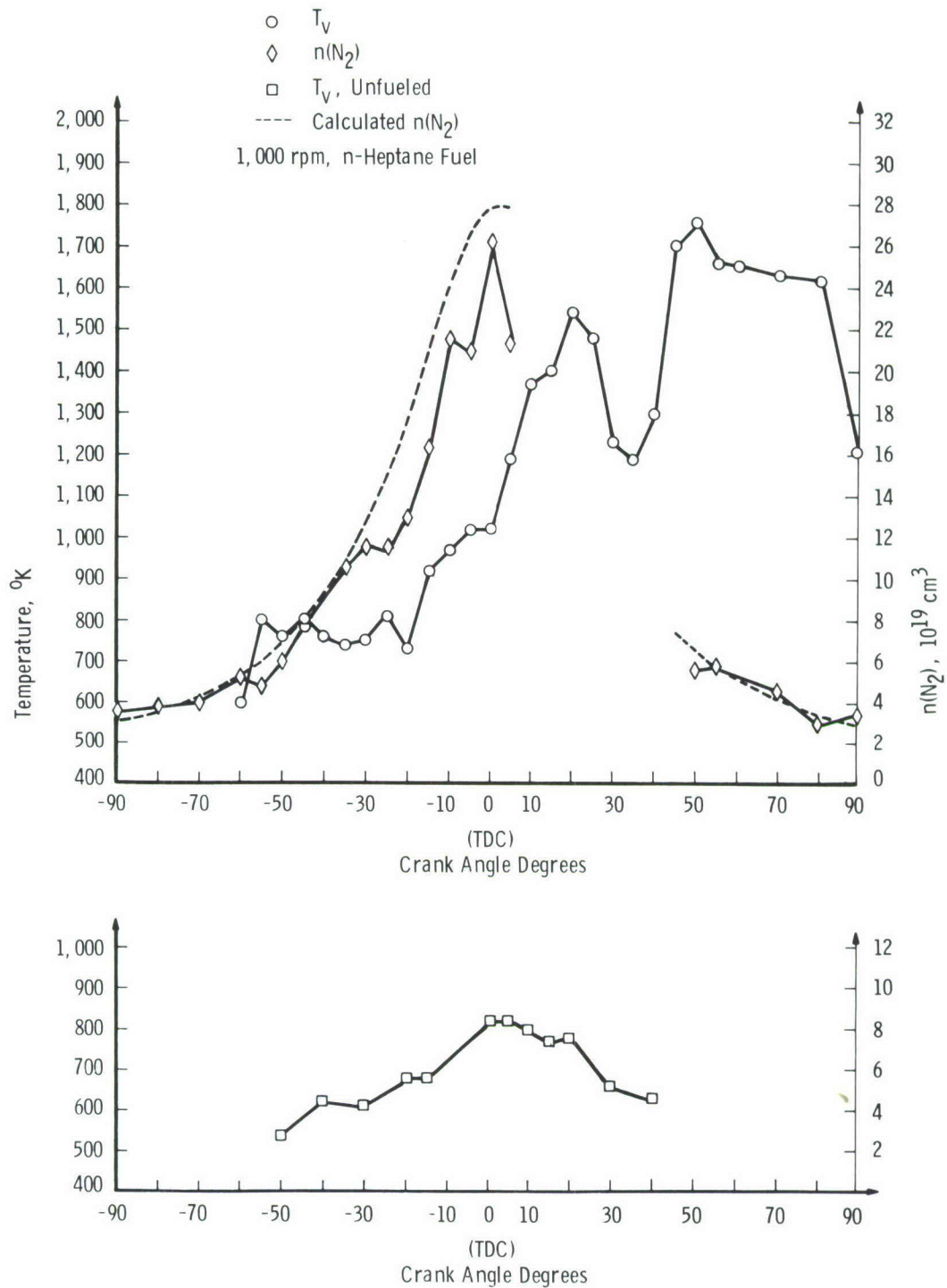


Figure 20. Temperature and N_2 number density as a function of CAD.

The evaluation of the intrinsic precision of the measurement process was made by using the photon counting error relations of Ref. 25, the error in the energy measurements, R_V (or R_r) and the $C_F(T, N_2)$ curves, and a Taylor's series method of error propagation. Although fueled mode measurements were made using a gated integrator rather than photon counting, the photons detected were estimated using the known gains of the photomultipliers and the sensitivity of the gated integrator. The precision, $S(T)$, of the temperature measurements was calculated to be ~ 5 percent, and the precision $S(n)$, of the N_2 number density was calculated to be ~ 4 percent.

The complete evaluation of total data uncertainty is impossible for several reasons. The variable effects of soot accumulation on the viewports during data acquisition cannot be estimated and the correlations between density and temperature fluctuations are unknown. Additionally, the temperature measurement depends on the accuracy of the theoretical calculation of intensity ratio as a function of temperature. However, the molecular constants used in the calculations are very reliable, and, as shown in Ref. 18, the convolution calculation of the RASP predicts spectral band profiles in very close agreement with measured profiles. Measured ratios at atmospheric conditions agreed within one percent with the calculated ratios.

Only a minimum total fractional uncertainty $U(n/T)$ in the measured density and temperature, (n/T) , was estimated using the relation

$$U\left(\frac{n}{T}\right) = \pm \left[B\left(\frac{n}{T}\right) + t_{0.95} S\left(\frac{n}{T}\right) \right] \quad (20)$$

where $B(n/T)$ represents the fractional systematic error in the parameter (n/T) . For evaluation of $U(n/T)$ the following values were used:

$$B(T) = 0.01$$

$$B(n) = 0.10$$

$$S(T) = 0.05$$

$$S(n) = 0.04$$

$$T_{0.95} = 2$$

Therefore the estimated minimum measurement fractional uncertainties are

$$U(T) = 0.11$$

$$U(n) = 0.18$$

5.0 SUMMARY

Measurements of temperature and N_2 number density have been obtained in the compression/power portion of the cycle of a CI engine operating at 1,000 rpm using n-heptane fuel at a flow rate of 0.024 gm /cycle. A double-peaked temperature versus crank angle distribution was measured, with the first peak occurring at 20 deg ATDC. The N_2 number density values obtained in regions in which laser beam attenuation was 40 percent were within 20 percent of predicted values.

The success of these measurements was directly attributable to the high energy, frequency doubled, blue wavelength of the laser source. Laser-Raman scattering can be used as a CI diagnostic if the laser excitation lies in the blue-to-green spectral region. For the technique to be a more accurate diagnostic, several experimental changes should be made. Specifically, the use of a higher repetition rate laser system and multichannel detection system is recommended to permit essentially instantaneous, single shot measurements which could be averaged and corrected (see Ref. 17) to give true average values.

REFERENCES

1. Borman, G. T., Myers, P. S., and Uyehara, O. A. "Engine Simulation Studies." TR-11398, U. S. Army Tank Automotive Command, Warren, Michigan, March 1972.
2. Lederman, S. "Some Applications of Laser Diagnostics to Fluid Dynamics." Paper 76-21, AIAA 14th Aerospace Sciences Meeting, Washington, D. C., Jan. 26—28, 1976.
3. Andree, A. and Packernegg, S. J. "Ignition Conditions in Diesel Engines." SAE-Paper 690253, Detroit, Michigan, January 1969.
4. Pischinger, R. and Cartellieri, W. "Combustion System Parameters and Their Effect Upon Diesel Engine Exhaust Emissions." SAE-Paper 720756, Milwaukee, Wisconsin, 1972.
5. Packernegg, S. J. "Efficient and Clean Diesel Combustion." SAE-Paper 750787, Milwaukee, Wisconsin, 1975.
6. Rassweiler, G. M., and Withrow, L. "Flame Temperatures Vary with Knock and Combustion Chamber Position." *SAE Transactions*, Vol. 36, No. 4, April 1935, pp. 125-133.
7. Livengood, J. C., Taylor, C. F., and Wu, P. C. "Measurements of Gas Temperatures in an Engine by Velocity of Sound Method." *SAE Transactions*, Vol. 66, 1958, pp. 683-699.

8. Millar, G. H., Ueyhara, O. A., and Myers, P. S. "Practical Application of Engine Flame Temperature Measurements." *SAE Transactions*, Vol. 62, 1954, pp. 514-530.
9. Muzio, L. J., Smith, D. S., and Starkman, E. S. "Emission-Absorption Temperature Measurement in the Cylinder of a Spark Ignition Engine." *Combustion and Flame*, Vol. 18, No. 3, June 1972, pp. 315-319.
10. Final Summary Report, CRC Project No. CM-1-53, Coordinating Research Council, New York, 1960.
11. Taylor, C. F. and Taylor, E. S. *The Internal Combustion Engine*. International Textbook Co., Scranton, Pennsylvania, 1961. (Second Edition).
12. Setchell, R. E. "Initial Measurements Within an Internal Combustion Engine Using Raman Spectroscopy." Sandia Laboratories SAND78-1220, Albuquerque, New Mexico, August 1978.
13. Smith, J. R. "Pulsed Raman Measurements in a Stratified Charge Engine." *AIAA Journal*, Vol. 18, No. 1, January 1980, pp. 118-120.
14. Stenhouse, I. A., Williams, D. R., Cole, J. B., and Swords, M. D. "CARS Measurements in an Internal Combustion Engine." *Applied Optics*, Vol. 18, No. 22, 15 November 1979, pp. 3819-3825.
15. Anderson, A., ed. *The Raman Effect*. Vol. 2, Marcel Dekker, Inc., New York, 1973.
16. Long, D. A., *Raman Spectroscopy*. McGraw-Hill International Book Co., New York, 1976.
17. Williams, W. D., Powell, H. M., Price, L. L., and Smith, G. D. "Laser-Raman Measurements in a Ducted, Two-Stream, Subsonic H₂/Air Combustion Flow." AEDC-TR-79-74 (AD-A078112), December 1979.
18. Williams, W. D., Wagner, D. A., Powell, H. M., and Price, L. L. "Laser-Raman Flow-Field Diagnostics of Two Large Hypersonic Test Facilities." AEDC-TR-79-88 (AD-A078289), December 1979.
19. Williams, W. D., et al. "Exhaust Plume Gas Dynamic and Radiation Measurements on a 500-lbf-Thrust Liquid Rocket Engine at Simulated Flight Conditions, Part II: Laser-Raman/Mass Spectrometer Diagnostics." AEDC-TR-78-17 (AD-B027812L), May 1978.

20. Cottrell, T. L. and McCoubrey, J. C. *Molecular Energy Transfer in Gases*. Butterworths, London, 1961.
21. Hirschfelder, J. O., Curtiss, C. F., and Bird, R. B. *Molecular Theory of Gases and Liquids*. John Wiley and Sons, Inc., New York, 1964.
22. Drake, M. C., and Rosenblatt, G. M. "Rotational Raman Scattering from Premixed and Diffusion Flames." *Combustion and Flame*, Vol. 33, No. 2, October 1978, pp. 179-196.
23. Eckbreth, A. C. "Averaging Considerations for Pulsed, Laser Raman Signals from Turbulent Combustion Media." *Combustion and Flame*, Vol. 31, No. 3, 1978, pp. 231-237.
24. Lennert A. E., et al. "Electro-Optical Techniques for Diesel Engine Research." AEDC-TR-77-17 (AD-A039357), May 1977.
25. Beers, Y. *Introduction to the Theory of Error*. Addison-Wesley Publishing Co., Inc., Reading, Massachusetts, 1957 (Second Edition).

NOMENCLATURE

A	Area of piston face
B	Fractional systematic error
BDC	Bottom dead center piston position
CAD	Crank angle degrees
$C_F(N_2)$	Calibration factor for N_2 density determination
$C_F(T, N_2)$	Relative temperature dependence of the intensity of the N_2 vibration-rotation band, $v = 0$ Q-branch
CI	Compression ignition
D	Piston diameter
\overline{D}	Engine displacement
E_p, E_o, E_t	Laser energy at the pyroelectric detector, at the laser output, and at the observation volume, respectively
E_v	Energy of vibrational mode
$I(N_2, Q)$	Intensity of the N_2 vibration-rotation band Q-branch
ℓ'	Length of connecting rod
M	Molecular weight
$n(N_2)$	N_2 number density
PMT	Photomultiplier tube
R	Universal gas constant
r	Compression ratio
r'	Crank radius
RASP	Raman Spectral Program
RDA	Rubidium dihydrogen arsenate

R_R	Relative sensitivity of two photomultiplier tubes
R_r	Intensity ratio formed with pure rotational intensities
R_v	Intensity ratio formed with vibration-rotation band
s_o	Linear clearance of engine
S	Fractional random error
T, T_{tr}	Temperature and translational temperature, respectively, of gas
TDC	Top dead center piston position
T_R, T_v	Rotational and vibrational temperature, respectively
TTY	Teletype
U	Total fractional uncertainty
V_{max}	Maximum cylinder volume
$V(\theta)$	Cylinder volume as a function of crank angle
V_o, V_{min}	Minimum cylinder volume
X_i	Mole fraction of species i
Z_{10}	Vibrational transfer collision number
Z_c	Intermolecular elastic collision rate
γ	Specific heat ratio
θ	Crank angle
λ, λ_o	Wavelength and laser wavelength, respectively
σ	Intermolecular potential range parameter

τ	Characteristic time of engine
τ_v	Vibrational relaxation time
$\Omega^{(2,2)*}$	Collision integral
ω	Angular speed of engine

SUBSCRIPTS

m	Indicates a measured value
c	Indicates a calculated value
0,1	Indicates $v = 0$ and $v = 1$ Q-branches

SUPERSCRIPTS

t	Indicates the value of a parameter during engine operation
---	--